



**Calhoun: The NPS Institutional Archive**  
**DSpace Repository**

---

Theses and Dissertations

1. Thesis and Dissertation Collection, all items

---

1999-12

# Convection activities within the stratocumulus-topped boundary layer

Whisenant, Michelle K.

Monterey, California. Naval Postgraduate School

---

<http://hdl.handle.net/10945/13487>

*Downloaded from NPS Archive: Calhoun*



Calhoun is a project of the Dudley Knox Library at NPS, furthering the precepts and goals of open government and government transparency. All information contained herein has been approved for release by the NPS Public Affairs Officer.

**Dudley Knox Library / Naval Postgraduate School**  
**411 Dyer Road / 1 University Circle**  
**Monterey, California USA 93943**

<http://www.nps.edu/library>

**NAVAL POSTGRADUATE SCHOOL**  
**Monterey, California**



**THESIS**

**CONVECTIVE ACTIVITIES WITHIN THE STRATOCUMULUS-  
TOPPED BOUNDARY LAYER**

by

Michelle K. Whisenant

December 1999

Thesis Advisor:

Qing Wang

Approved for public release; distribution is unlimited.

20000309 020

**REPORT DOCUMENTATION PAGE**Form Approved  
OMB No. 0704-0188

Public reporting burden for this collection of information is estimated to average 1 hour per response, including the time for reviewing instructions, searching existing sources, gathering and maintaining the data needed, and completing and reviewing the collection of information. Send comments regarding this burden estimate or any other aspect of this collection of information, including suggestions for reducing this burden to Washington Headquarters Services, Directorate for Information Operations and Reports, 1215 Jefferson Davis Highway Suite 1204, Arlington, VA 22202-4312, and to the Office of Management and Budget, Paperwork Reduction Project (0704-0188), Washington, DC 20503.

|   |  |   |   |  |
|---|--|---|---|--|
| 1. AGENCY USE ONLY (Leave blank)  |  | 2. REPORT DATE<br>December 1999                         | 3. REPORT TYPE AND DATES COVERED<br>Master's Thesis |  |
| 4. TITLE AND SUBTITLE<br>CONVECTIVE ACTIVITIES WITHIN THE STRATOCUMULUS-TOPPED BOUNDARY LAYER   |  |   | 5. FUNDING NUMBERS                                  |  |
| 6. AUTHOR(S)<br>Michelle K. Whisenhant  |  |   |   |  |
| 7. PERFORMING ORGANIZATION NAME(S) AND ADDRESS(ES)<br>Naval Postgraduate School<br>Monterey, CA 93943-5000  |  |   | 8. PERFORMING ORGANIZATION REPORT NUMBER            |  |
| 9. SPONSORING/MONITORING AGENCY NAME(S) AND ADDRESS(ES)   |  |   | 10. SPONSORING/MONITORING AGENCY REPORT NUMBER      |  |
| 11. SUPPLEMENTARY NOTES<br>The views expressed in this thesis are those of the author and do not reflect the official policy or position of the Department of Defense or the U.S. Government.   |  |   |   |  |
| 12a. DISTRIBUTION/AVAILABILITY STATEMENT<br>Approved for public release; distribution is unlimited.   |  |   | 12b. DISTRIBUTION CODE                              |  |
| 13. ABSTRACT (Maximum 200 words)<br>This study utilizes aircraft measurements obtained off the California coast to analyze the geometric, thermodynamic, and microphysical characteristics of convective updrafts and downdrafts in the stratocumulus-topped boundary layer (BL). The vertical structure of thermodynamic and microphysical properties is consistent. The difference in peak droplet concentration between updrafts, downdrafts, and the defined environment increases near the cloud top. We observe larger mean droplet diameters in downdrafts near the cloud top, as the number of small droplets in cloud top downdrafts appears to decrease. The horizontal variability seen in the cloud droplet spectra and microphysics properties is likely due to aerosol activation and growth in updrafts, cloud top entrainment, and penetrating cumulus. We compute the mass flux, $\omega^*$ , using a mass flux parameterization. Several measured variables produce consistent results and agree with mass flux calculations from other stratocumulus datasets. |  |   |   |  |
| 14. SUBJECT TERMS<br>Convective Events, Cloud Microphysics, Stratocumulus-Topped Boundary Layer, FIRE.  |  |   | 15. NUMBER OF PAGES<br>96                           |  |
|   |  |   | 16. PRICE CODE                                      |  |
| 17. SECURITY CLASSIFICATION OF REPORT<br>Unclassified   | 18. SECURITY CLASSIFICATION OF THIS PAGE<br>Unclassified | 18. SECURITY CLASSIFICATION OF ABSTRACT<br>Unclassified | 20. LIMITATION OF ABSTRACT<br>UL                    |  |

NSN 7540-01-280-5500

Standard Form 298 (Rev 2-89)  
Prescribed by ANSI Std. Z39-18  
298-102

THIS PAGE INTENTIONALLY LEFT BLANK

Approved for public release; distribution is unlimited

**CONVECTIVE ACTIVITIES WITHIN THE STRATOCUMULUS-TOPPED  
BOUNDARY LAYER**

Michelle K. Whisenant  
Lieutenant, United States Navy  
B.S., Florida Institute of Technology, 1990

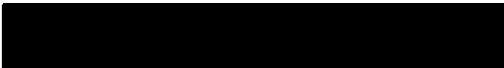
Submitted in partial fulfillment of the  
requirements for the degree of

**MASTER OF SCIENCE IN METEOROLOGY AND  
PHYSICAL OCEANOGRAPHY**

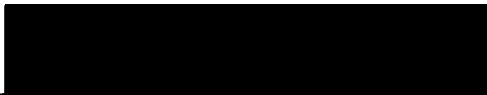
from the

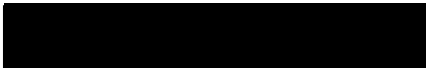
**NAVAL POSTGRADUATE SCHOOL  
December 1999**

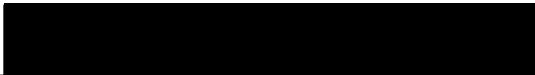
Author:

  
Michelle K. Whisenant

Approved by:

  
Qing Wang, Thesis Advisor

  
Peter S. Guest, Second Reader

  
Robert L. Haney, Chairman  
Department of Meteorology

THIS PAGE INTENTIONALLY LEFT BLANK

## ABSTRACT

This study utilizes aircraft measurements obtained off the California coast to analyze the geometric, thermodynamic, and microphysical characteristics of convective updrafts and downdrafts in the stratocumulus-topped boundary layer (BL). The vertical structure of thermodynamic and microphysical properties is consistent. The difference in peak droplet concentration between updrafts, downdrafts, and the defined environment increases near the cloud top. We observe larger mean droplet diameters in downdrafts near the cloud top, as the number of small droplets in cloud top downdrafts appears to decrease. The horizontal variability seen in the cloud droplet spectra and microphysics properties is likely due to aerosol activation and growth in updrafts, cloud top entrainment, and penetrating cumulus. We compute the mass flux,  $\omega^*$ , using a mass flux parameterization. Several measured variables produce consistent results and agree with mass flux calculations from other stratocumulus datasets.

THIS PAGE INTENTIONALLY LEFT BLANK



## TABLE OF CONTENTS

|      |  |    |
|------|--|----|
| I.   | INTRODUCTION .....   | 1  |
| A.   | IMPORTANCE OF STRATOCUMULUS CLOUDS TO WORLD<br>CLIMATE AND TO NAVAL OPERATIONS ..... | 1  |
| B.   | PHYSICAL PROCESSES IN STRATOCUMULUS-TOPPED<br>BOUNDARY LAYERS .....                  | 2  |
| C.   | OBJECTIVES .....   | 5  |
| II.  | OVERVIEW OF THE EXPERIMENT AND THE DATA .....  | 9  |
| A.   | OVERVIEW OF THE EXPERIMENT .....   | 9  |
| B.   | AIRCRAFT AND INSTRUMENTATION .....   | 10 |
| C.   | DATA SELECTION .....   | 12 |
| D.   | SUMMARY OF FLIGHT CONDITIONS .....   | 13 |
| III. | GEOMETRIC PROPERTIES OF CONVECTIVE EVENTS .....                                      | 27 |
| A.   | CONDITIONAL SAMPLING METHOD .....  | 27 |
| B.   | GEOMETRIC CHARACTERISTICS OF EVENTS .....  | 30 |
| IV.  | THERMODYNAMIC AND MICROPHYSICAL PROPERTIES OF<br>CONVECTIVE EVENTS .....             | 41 |
| A.   | THERMODYNAMIC PROPERTIES .....   | 41 |
| B.   | MICROPHYSICAL PROPERTIES .....   | 55 |
| C.   | CONVECTIVE MASS FLUX PARAMETRIZATION .....   | 71 |
| V.   | SUMMARY, CONCLUSIONS, AND DISCUSSION .....   | 75 |
| A.   | SUMMARY AND CONCLUSIONS .....  | 75 |
| B.   | DISCUSSION .....   | 78 |
|      | LIST OF REFERENCES .....   | 81 |
|      | INITIAL DISTRIBUTION LIST .....  | 85 |

THIS PAGE INTENTIONALLY LEFT BLANK

## ACKNOWLEDGEMENTS

I would like to sincerely thank my advisor, Dr. Qing Wang, of the Department of Meteorology, Naval Postgraduate School, for her patience, guidance and support throughout the development of my thesis. Additionally, I thank Dr. Peter Guest for his helpful comments as the second reader.

The following Department of Meteorology, Naval Postgraduate School personnel were also of great assistance at various stages in my research: Dr. Phil Durkee, Mr. Kurt Nielsen, Ms. Mary Jordan, Mr. Russ Schwanz, Mr. Bill Thompson, and Mr. Bob Creasey.

I also thank my husband, Rob, for keeping me smiling and laughing, and the great sport of cycling, for keeping me sane and healthy, during my studies at the Naval Postgraduate School.

THIS PAGE INTENTIONALLY LEFT BLANK

## I. INTRODUCTION

### A. IMPORTANCE OF STRATOCUMULUS CLOUDS TO WORLD CLIMATE AND TO NAVAL OPERATIONS

It is estimated that marine stratocumulus clouds cover about 25% of the world's oceans at any time (Kogan et al. 1995), particularly along the west coasts of continents under the influence of subtropical high pressure and large scale subsidence inversions. The reflectivity of solar radiation at the cloud top is much higher than that of the ocean surface, therefore, solar energy reaching the surface is significantly reduced in the presence of stratocumulus. Stratocumulus clouds emit long-wave radiation at nearly the same temperature as the ocean surface due to their low altitude and hence do not greatly affect the infrared radiation emitted to space. Consequently, the presence of stratocumulus clouds result in reduction of the net radiation received, and thus a net cooling of the earth system. (Kogan et al. 1995) estimate that an increase of a few percent of low cloud cover would counter the greenhouse warming effect, while similar decreases would double the warming. Thus it is apparent that, from a climate-modeling perspective, the understanding and accurate representation of these clouds in climate models is important.

The structure and evolution of the cloud-topped boundary layer (BL) are also important to the United States Navy, both from a tactical and meteorological standpoint. A cloud-topped BL adds a level of complexity and uncertainty in assessing and predicting BL structure, potentially degrading environmental forecasts and the effectiveness of

tactical decisions. The presence of stratocumulus, for example, significantly alters the BL inversion strength, which plays a role in electromagnetic and electro-optical propagation and the tactical evaluation of elevated ducts. The change in inversion strength and corresponding changes in cloud evolution also modifies aerosol-cloud interaction. The resulting changes to cloud structure therefore impact Navy remote sensing and surveillance capability, such as in the satellite analysis of ship tracks. The presence of stratocumulus also adds difficulty to short-term and mesoscale forecasting. Consequently, an improved understanding of the evolution of a stratocumulus-topped BL could significantly enhance the Navy's tactical use of the environment.

#### **B. PHYSICAL PROCESSES IN STRATOCUMULUS-TOPPED BOUNDARY LAYERS**

Figure 1 illustrates the major physical processes in the stratocumulus-topped BL. One of the physical processes is long-wave radiative cooling at the cloud top. The vertical extent of this cooling is limited to a shallow region adjacent to the cloud top. This strong cooling generates cold downdrafts descending from the cloud top and compensating warm updrafts, resulting in positive buoyancy flux near the cloud top. This radiative cooling is therefore an important source for turbulence. Another important process in the cloudy BL is entrainment near the cloud top, where turbulence in the BL mixes air from above the inversion into the BL. Because the entrained air is typically warmer and drier than BL air, entrainment mixing may result in evaporation of the cloud droplets and thus

evaporative cooling. This process, under certain circumstances, modifies the BL and cloud structure as discussed in Randall (1980), Siems et al. (1990), Wang and Albrecht (1994), and others.

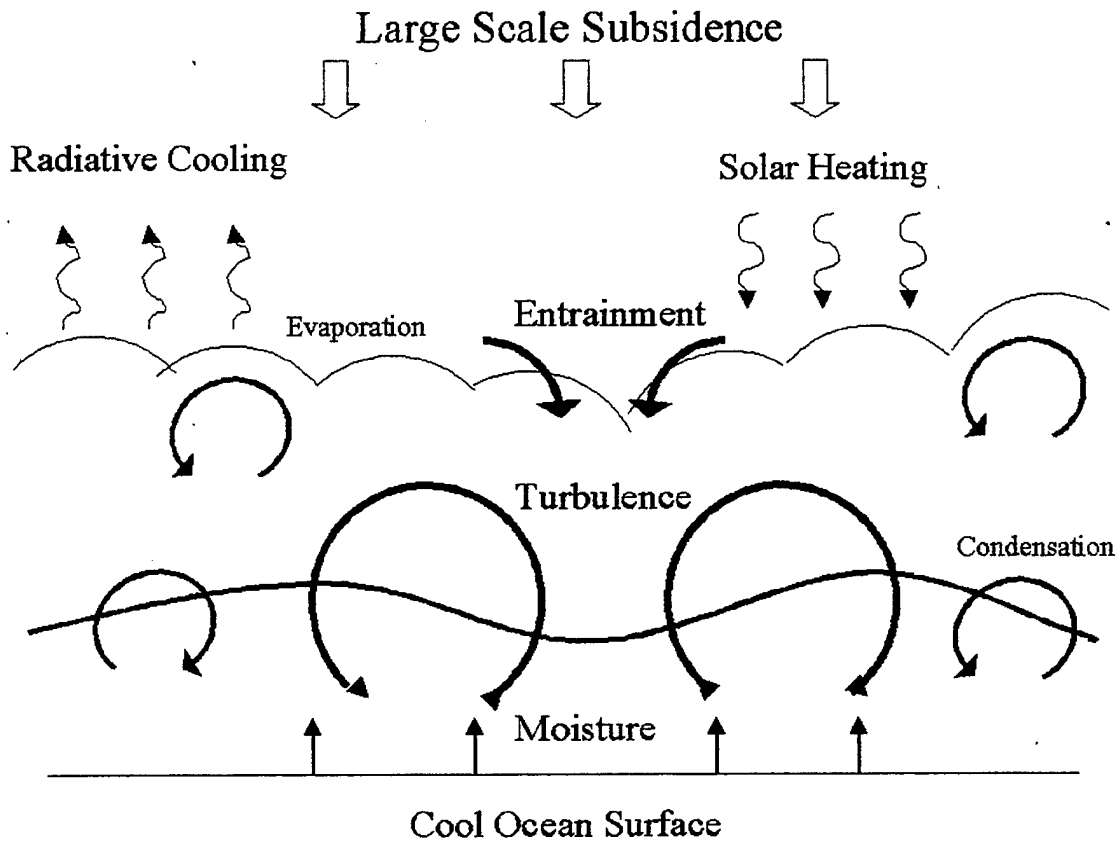


**Figure 1.** Physical Processes in the Marine Stratocumulus-topped BL.

Heating from absorption of short-wave solar energy also occurs in the cloud layer. In contrast to the long-wave cooling, this heating is distributed more evenly in the cloud layer (Fravallo et al. 1981). In addition, infrared

(IR) radiation also results in a small amount of warming near the cloud base (Fravalo et al. 1981). The net result of both solar and IR radiation heating is to warm the cloud layer relative to the sub-cloud layer, forming a stable layer near the cloud base. This leads to a separation of the upper BL (including cloud layer) from the layer below, prohibiting vertical transport between the two layers. This phenomenon is referred to as decoupling. When decoupling happens, the supply of moisture to the cloud is reduced, and enhanced thinning of the cloud may occur.

The ocean surface is always a source of water vapor to maintain the cloud layer. However, the buoyancy effect of the ocean surface on the cloud-topped BL is rather uncertain because of the small air-sea temperature difference. The following chapters will present results from different flights that show the variability created by this effect. In addition to buoyancy, vertical shear of the mean wind speed near the surface and the cloud top modifies the dynamics of the cloudy BL.

The dynamic processes within the stratocumulus cloud can cause vertical and horizontal variations in the droplet spectra. For example, in regions of dry air entrainment and associated downdrafts at the cloud top, droplet concentrations may be less than in the updraft regions, due to evaporation. Many studies (Rogers and Telford 1986, Nicholls 1989, Khalsa 1993, and Wang and Lenschow 1995) have found narrow regions of lower than average liquid water content near the stratocumulus cloud top, attributed to entrainment of dry air. Gerber (1996) calculated the effective radius of droplets inside and outside regions of depleted liquid water content near the cloud top and found little change in the relative size distribution between the



two regions. This finding supports the suggestion of Nicholls and Leighton (1986) that entrainment at the cloud top does not effect the shape of the spectrum, but only acts to dilute the droplet concentration.

Conversely, due to radiative cooling and other processes at the cloud top, pockets of high supersaturation can exist, creating a region of higher cloud droplet concentration (Kogan et al. 1995). Updraft regions in decoupled BLs often show a bimodal distribution, especially near the cloud base, as air parcels descending from the cloud top are strongly decelerated and can be recaptured by updrafts near the cloud base and recycled (Kogan et al. 1995).

### **C. OBJECTIVES**

The general dynamics of marine stratocumulus have been extensively researched, but the dynamics and microphysics in relation to the convective activities in these clouds are relatively unexplored. One subject is the role of in-cloud updrafts and downdrafts in determining the horizontal structure of the cloud and in altering droplet distributions within the cloud. The vertical motions within cumulus clouds are roughly an order of magnitude larger than in stratocumulus clouds, but even though the vertical motions are weaker, there are apparent differences between microphysical and dynamical parameters in stratocumulus updrafts and downdrafts. Understanding the relationships between cloud microphysics, dynamics, and radiative properties is an important step in the accurate modeling of stratocumulus development, with cloud updrafts and downdrafts being the important link between these

properties. This understanding is dependent on the acquisition and analysis of data capturing these important quantities, but few observational studies have made these necessary comprehensive measurements.

Most numerical models of stratocumulus clouds employ a bulk parameterization of cloud microphysics, rather than explicit resolution of cloud droplet size distributions. The former saves a large amount of computer time, but at the expense of accuracy and loss of potentially important physical effects. Advancement in microphysics formulations may be critical for improving prediction of stratocumulus evolution. Kogan et al. (1995) employ explicit formulation of microphysical processes in a large eddy simulation model of stratocumulus, and demonstrate that cloud microphysical parameters are significantly affected by cloud dynamics, and that the cloud microstructure is significantly asymmetric between updrafts and downdrafts. The resultant mixing due to the updraft/downdraft plumes causes variability in the cloud layer structure, especially near the cloud top and base.

This study intends to describe the significant horizontal variability associated with the turbulent updrafts and downdrafts within the stratocumulus-topped BL. We will analyze the characteristics of the convective events and the role of updrafts and downdrafts on both the thermodynamic and microphysical structure of the BL using a comprehensive data set. This analysis will provide additional understanding of the relationships between the cloud microphysical structure and the dynamic structure, for improvement of numerical modeling of these clouds in large eddy simulations and higher order closure models.

This thesis is organized into five chapters. Chapter II describes the experiment and the data used in the analysis.

Chapter III provides a detailed analysis of updraft and downdraft events within the stratocumulus-topped BL. Chapter IV discusses the microphysical and thermodynamic properties within the updrafts and downdrafts, and discusses the validity of mass flux parameterization in the stratocumulus-topped BL. Chapter V contains the summary and conclusions.

THIS PAGE INTENTIONALLY LEFT BLANK

## II. OVERVIEW OF THE EXPERIMENT AND THE DATA

### A. OVERVIEW OF THE EXPERIMENT

During June and July 1987, the First International Satellite Cloud and Climate Project (ISCCP) Regional Experiment (FIRE) Marine Stratocumulus Intensive Field Observations (IFO) was conducted off the coast of southern California. FIRE obtained a comprehensive set of measurements using 12 coordinated multi-missions with five separate research aircraft, surface-based measurements, and satellite imagery. One of the main objectives of FIRE was to provide observations that would test theories on the development, maintenance, and dissipation of marine stratocumulus clouds. The knowledge gained could be used to improve cloud parameterizations used in large-scale models and to develop and test satellite cloud-retrieval schemes.

Albrecht et al. (1988) and Cox et al. (1987) give a detailed description of project objectives. In addition, Kloesel et al. (1988) gives a summary of experiment operations and general meteorological conditions during the period. A later section will briefly describe each flight analyzed in this thesis. In this study, we utilize data obtained by the NCAR Electra aircraft in seven of the ten flights flown during FIRE to analyze various aspects of the spatial variability in the cloudy BL. The seven flights chosen to study contain horizontal turbulence leg data at levels both in and out of the cloud (flights 2, 3, 4, 6, 7,

8 and 9). McDowell (1999) gives the general locations of each of the ten Electra flights.

## **B. AIRCRAFT AND INSTRUMENTATION**

The National Center for Atmospheric Research (NCAR) Electra aircraft made turbulence, radiation, and cloud microphysics measurements in the BL. Each Electra mission consisted of horizontal legs at different altitudes in and above the marine BL, and vertical soundings throughout the BL. The aircraft speed was held constant at  $100 \text{ m s}^{-1}$ . Horizontal flight legs consisted of 20-minute L-shaped legs at levels in, above, and below the cloud layer, and one level near the surface. These legs captured cloud structure and measured the turbulent flux profiles at various levels in the BL. Slant path or spiral soundings at multiple time periods and locations provided vertical profiles of BL variations, inversion layer characteristics, and a representation of the air properties above the BL. These soundings were treated as vertical profiles assuming near horizontal homogeneity. A typical flight track of the Electra measurement is shown in Figure 2.

Measurements utilized in this thesis work include cloud droplet size distribution, temperature, horizontal and vertical wind velocity, water vapor specific humidity, liquid water content, and ozone concentration. Most of the data was sampled at a 50 Hz sampling rate and recorded at 20 Hz for data processing. The 20 Hz data are used for analysis in this study. McDowell (1999) describes the Electra instruments used in obtaining these data

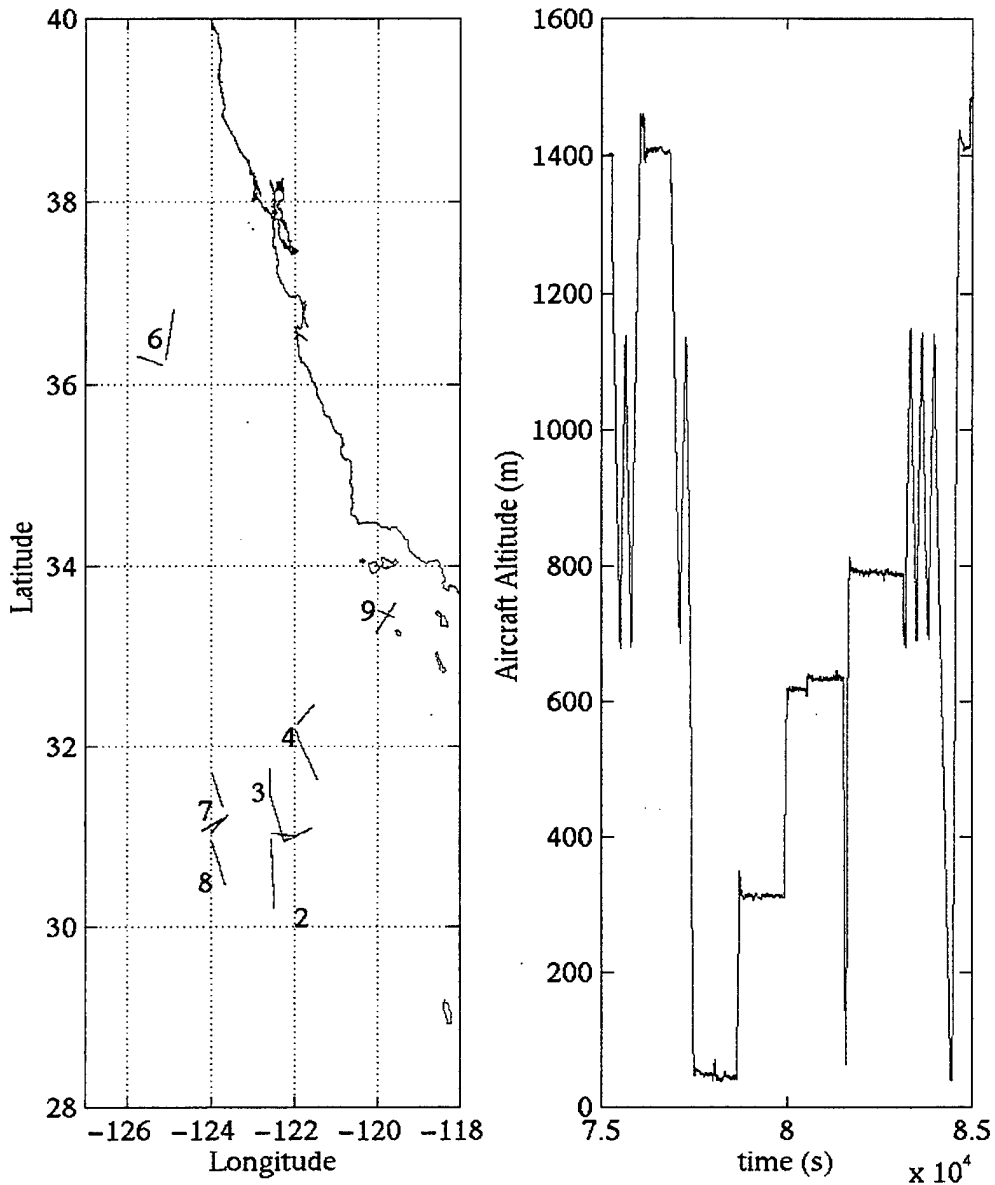


**Figure 2.** Example from FIRE Flight 2. Left: the flight path of the NCAR Electra during the horizontal turbulence legs. Right: the time variation in aircraft altitude for one flight segment, showing the order of the vertical soundings and horizontal turbulence leg measurements.

except for the ones described below.

The Particle Measuring Systems (PMS) Forward Scattering Spectrometer Probe (FSSP) measures concentration and droplet size in the 3-45 micron range. The FSSP is an optical particle counter (OPC) that detects single particles and sizes them by measuring the intensity of light that the particle scatters when passing through a light beam. The Mie scattering theory is used to relate the intensity to the particle size. The size is categorized into one of 15 channels, each covering a 3 micrometers range. This study utilizes this cloud droplet size distribution to generate droplet spectra at different vertical levels and in updrafts and downdrafts within the cloud.

A Rosemount 858 probe, a flow angle sensor that accounts for aircraft attack angle and sideslip, measured the wind velocities used in this study.

### **C. DATA SELECTION**

Horizontal flight legs at different levels within and below cloud were used to analyze the variation in BL and cloud characteristics at different altitudes within the cloud. In general, the horizontal turbulence legs were identified using aircraft altitude and heading data. A horizontal turbulence leg was defined for each time segment when the aircraft was at both a constant altitude and heading. The in-cloud legs were identified as time segments within those horizontal legs where the aircraft measured a significant droplet concentration. Flight log



entries and soundings done in the vicinity of the horizontal legs were used to determine the cloud boundaries and BL heights used to scale the altitudes of the horizontal measurements to be presented in the later chapters.

#### **D. SUMMARY OF FLIGHT CONDITIONS**

The following section will give a brief description of the BL meteorological conditions of the seven FIRE flights analyzed in this study based on information from Kloesel et al. (1988) and Laufersweiler and Kloesel (1991). The general turbulence structure in each flight will also be discussed. These discussions will be important in explaining the differences seen in the cloud dynamics and microphysics in the data analysis contained in later chapters.

##### **1. Meteorological Conditions**

The following is a brief summary of the synoptic and BL meteorological conditions for each of the FIRE flights analyzed in this study. Table 1 lists the flight date, time, average BL depth, maximum liquid water content, and cloud depth for each flight.

Measurements of flight 2 were taken from late morning to mid-afternoon. An intensified Pacific subtropical high to the north and an inland thermal low created northwesterly winds in the project area. The winds in the BL averaged 3 to 5 m s<sup>-1</sup>, relatively weak in comparison to the other flights. The flight began with large cloud areas

with some breaks, but by the end of the mission, a nearly solid cloud deck was observed in the operation region. The horizontal in-cloud turbulence legs were flown in a mix of thin, broken, and solid cloud. Broken cumulus was also observed beneath the stratocumulus deck, with some cumulus extending upwards into the stratocumulus. Drizzle was also observed at various times during the flight.

**Table 1.** Flight and Boundary Layer Information for the Seven Flights Analyzed in this Study.

| Flt # | Date    | Start/End Time (UTC) | Average BL Depth (m) | Average Cloud Depth (m) | BL max $q_1$ |
|-------|---------|----------------------|----------------------|-------------------------|--------------|
| 2     | 6/30/87 | 1854/2348            | 896                  | 300                     | .33          |
| 3     | 7/3/87  | 0116/0604            | 890                  | 322                     | .31          |
| 4     | 7/5/87  | 1743/2304            | 904                  | 283                     | .30          |
| 6     | 7/10/87 | 1855/2313            | 751                  | 383                     | .32          |
| 7     | 7/11/87 | 1727/2137            | 895                  | 395                     | .33          |
| 8     | 7/14/87 | 1800/2315            | 811                  | 371                     | .40          |
| 9     | 7/16/87 | 1625/1951            | 829                  | *                       | .28          |

\*Widely varied due to complex cloud conditions.

Measurements for flight 3 began in late afternoon. A relatively weak Pacific subtropical high and weak thermal low east of the Baja Peninsula created generally northerly winds ( $7$  to  $10 \text{ m s}^{-1}$ ) that were much stronger than for flight 2. The BL in the measurement area was covered by

nearly solid cloud with some thin breaks, with a large clear area to the west. As measurements continued well into hours of darkness, the cloud deck became very solid. The bases of the stratocumulus were ragged and the tops were variable and undulating. No lower cumulus layer was evident and very little drizzle was observed.

Measurements for flight 4 started in the late morning and continued into the mid-afternoon. The persistent Pacific subtropical high and inland thermal low created rather strong north-northwesterly surface winds (8 to 13 m s<sup>-1</sup>) in the measurement area on this day. A thin, solid stratocumulus deck existed, which became more broken later in the flight. No precipitation or lower cumulus was evident.

Flight 6 took place off of the central California coast. Measurements started around local noon and continued into the mid-afternoon. The Pacific subtropical high had moved slightly westward, weakening the pressure gradient over the measurement area and creating moderate north-northwesterly surface winds. A mix of thin, solid and broken stratocumulus existed. Later in the flight, the stratocumulus became more solid, the inversion was relatively higher, and the cloud bases became variable, with some reported cloud bases as low as 100 m. All of the in-cloud horizontal turbulence legs analyzed in flight 6 were from this later segment. No precipitation or lower cumulus was evident during the turbulence legs.

Measurements for flight 7 started around 1100 local time and continued into the mid-afternoon. The Pacific subtropical high remained in nearly the same position as

the previous day, while the inland thermal low weakened. This created a weaker pressure gradient and thus weaker winds out of the north-northwest in the measurement area. Cloud conditions were similar to flight 2 with a mix of thin, broken, and solid cloud, and an extensive lower cumulus layer with some cumulus extending upwards into the stratocumulus. The lower cumulus appeared to be suppressed in areas where the stratocumulus was thin or broken. Numerous showers were observed during the turbulence legs.

Flight 8 also started in the late morning and continued into the mid-afternoon. The subtropical high had moved farther north and east than in previous flights and the inland thermal low strengthened producing strong northwesterly winds ( $7$  to  $10 \text{ m s}^{-1}$ ) in the project area. A relatively solid and thick cloud deck covered about half of the BL depth, which became slightly more broken later in the flight. A lower cumulus layer also existed, which in some cases extended up into the stratocumulus deck. Some drizzle was also observed.

Measurements for flight 9 started around 0830 local time and continued until around noon local time. Although the subtropical high and the inland thermal low both strengthened from the previous day, the pressure gradient and winds over the project area remained relatively unchanged. Flight 9 was conducted in the vicinity of San Nicholas Island within the southern California bight. All other flights were conducted much farther from land over the open ocean. This was likely a major factor in the dramatic differences in BL cloud conditions seen in this flight, which were by far the most complex of all the FIRE

flights. At times three cloud decks existed: two stratocumulus decks at different vertical levels, varying from solid to broken, and a lower cumulus field. Showers and fog were also observed.

It is seen from Table 1 that all measurements, except flight 3, were made during the daytime. The BL height, the cloud depth, and the maximum liquid water content are comparable in all flights.

## **2. Boundary Layer Mean and Turbulence Structure**

An example of the BL vertical structure from aircraft soundings is shown in Figure 3. This sounding is typical of the stratocumulus-topped BLs analyzed in this study. Here, the BL, as indicated by the virtual potential temperature profile (Figure 3a), is approximately 800 m deep, capped by a sharp temperature inversion. The number concentration of droplets (Figure 3c) remains fairly constant throughout the roughly 500 m depth of the cloud deck. The average diameter of droplets (Figure 3d) increases with height within the cloud, and liquid water content (Figure 3b) increases smoothly with height, reaching a maximum at the cloud top. Note that readings of droplet size below the cloud base are due to instrument noise and are therefore erroneous.

Table 2 lists values of the surface buoyancy flux, surface frictional velocity ( $u^*$ ), and the cloud layer convective velocity scale ( $w^*c$ ), which are used to

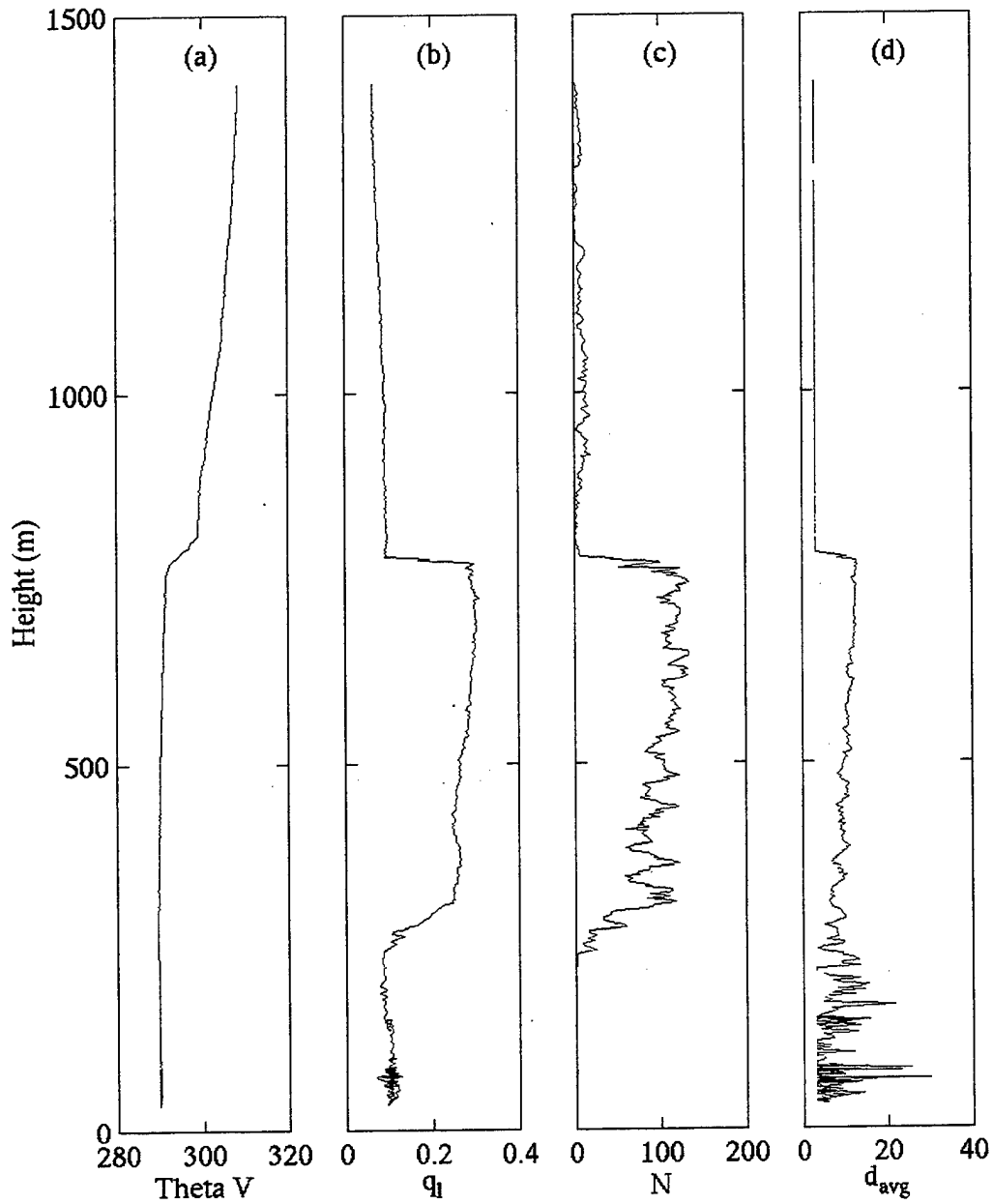


**Figure 3.** Typical Vertical Profiles in Stratocumulus-topped Boundary Layers. (a) virtual potential temperature (K), (b) liquid water content ( $\text{g kg}^{-1}$ ), (c) droplet concentration ( $\text{cm}^{-3}$ ), and (d) average droplet diameter ( $\mu\text{m}$ ). The measurements are from FIRE flight 9 on 16 July 1987.

characterize the source of turbulence in the BL. The convective velocity is defined using the buoyancy flux profiles in the cloud mixed layer following the method in Deardorff (1980):

$$w_{*c} = \{2.5(g/\bar{\theta}_v) \int_{z_0}^{z_i} \overline{w'\theta'_v} dz\}^{1/3}, \quad (1)$$

where  $\bar{\theta}_v$  is the average virtual potential temperature in the layer of integration,  $\overline{w'\theta'_v}$  is the buoyancy flux calculated from direct eddy correlation method (Stull 1988), and  $g$  is the gravitational acceleration. The lower limit of the integration,  $z_0$ , is the altitude at which buoyancy flux is zero which is assumed at the base of the cloud mixed layer. The upper limit,  $z_i$ , is the cloud-top height. These limits are similar to those used by Deardorff, except that his lower limit,  $z_0$ , is the height of the cloud mixed layer base for decoupled cases, and 0 for well-mixed cases. The convective velocity thus defined indicates the forcing due to radiative cooling and other processes at the cloud top. The frictional velocity is defined as (Brost et al. 1982):

$$u_* = (\overline{w'v'^2} + \overline{w'u'^2})^{1/4}, \quad (2)$$

where  $\overline{w'v'}$  and  $\overline{w'u'}$  are the momentum fluxes for the north-south and east-west wind components, respectively.  $u_*$  therefore denotes the magnitude of the wind shear near the surface.

The extent of vertical turbulent mixing is qualitatively defined as a decoupled or a well-mixed BL in Table 2. The definition is based upon the comparison

between the lidar-measured cloud-base height and the lifting condensation level (LCL) calculated using measurements from the lowest flight legs. In cases where the lidar cloud base height was unavailable, signatures of layer separation from the sounding profiles are used. The results in Table 2 for flights 2, 3, 4, and 8 are from Wang (1993). The same method was used for the rest of the flights. Flight 7 was classified as decoupled, since the LCL and cloud-base height were not in good agreement. Since the lidar was inoperable during flight 6, soundings were inspected for evidence of a transition layer. The vertical profiles of moisture and potential temperature indicate a well-mixed BL, and the LCL and cloud base heights estimated from liquid water and droplet concentration jumps in sounding data are in fairly good agreement. The BL structure for flight 6 will therefore be classified as well-mixed. Flight 9 illustrates the potential variability and complexity of near-coastal stratocumulus-topped BLs. The complexity is suggested by the BL cloud structure as described earlier. There is significant scatter in the TKE and turbulence flux throughout the BL. The low value of surface buoyancy flux is a result of the averaging of both positive and negative near-surface flux values, indicating significant horizontal variability in the near-surface conditions. This scatter, coupled with the relatively smaller amount of data collected during the horizontal turbulence legs, makes classification of the BL during flight 9 difficult.



**Table 2** Buoyancy and Shear Forcing and Mean Turbulent Kinetic Energy (TKE) for each Flight. The surface buoyancy flux is in  $W m^{-2}$ , surface friction velocity is in  $m s^{-1}$ , cloud layer convective velocity is in  $m s^{-1}$ , the production rate of near surface buoyancy and shear-generated TKE are in  $m^2 s^{-3}$  and BL averaged TKE are in  $m^2 s^{-2}$ .

| Flt # | Production rate of near-surface Buoyancy-generated TKE ( $\times 10^{-4}$ ) | Production rate of near-surface Shear-generated TKE ( $\times 10^{-4}$ ) | Near-surface $u_*$ | Cloud layer $w_{*c}$ | BL TKE <sub>avg</sub> | BL Turbulent Mixing |
|-------|---|--|--------------------|----------------------|-----------------------|---------------------|
| 2     | 2.04  | 0.14   | 0.16               | 0.35                 | 0.40                  | decoupled           |
| 3     | 1.32  | 55.0   | 0.25               | 0.75                 | 0.93                  | well-mixed          |
| 4     | 2.17  | 30.7   | 0.40               | 0.38                 | 0.60                  | well-mixed          |
| 6     | -2.34   | 24.5   | 0.34               | 0.32                 | 0.41                  | well-mixed          |
| 7     | 3.55  | 0.70   | 0.26               | 0.03                 | 0.50                  | decoupled           |
| 8     | 5.10  | 14.8   | 0.38               | 0.21                 | 0.38                  | decoupled           |
| 9     | 0.547   | 2.80   | 0.24               | *                    | 0.52                  | *                   |

\* Structure of turbulent mixing is not clearly defined.

Following Wang et al. (1999), the upper BL associated with the cloud layer will be referred to as the cloud mixed layer, while the lower layer will be called the surface-based layer.

Vertical profiles of TKE from all seven flights are shown in Figure 4 to aid the discussion of turbulent structure. The BL mean TKE is given in Table 2, and indicates that two of the well-mixed cases (flights 3 and

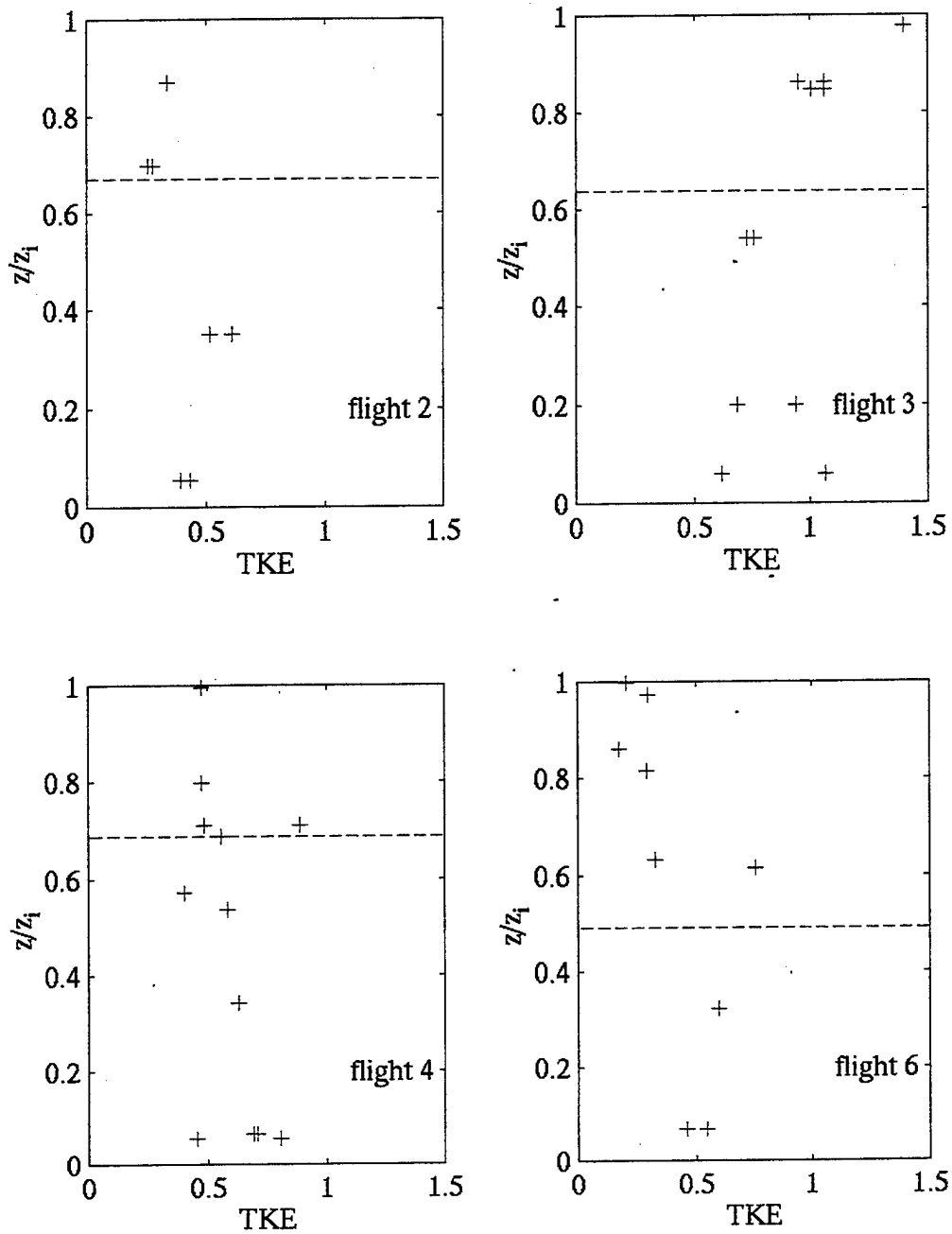


**Figure 4.** Vertical profiles of TKE for all Seven Flights. The horizontal axes are TKE in  $\text{m}^2\text{s}^{-2}$ , the vertical axes are height,  $z$ , scaled by the boundary layer depth,  $z_1$  (Table 1). The dotted line shows the average height of the cloud base.

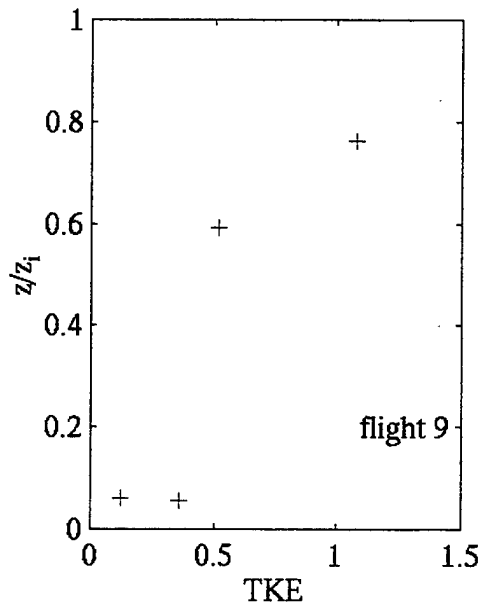
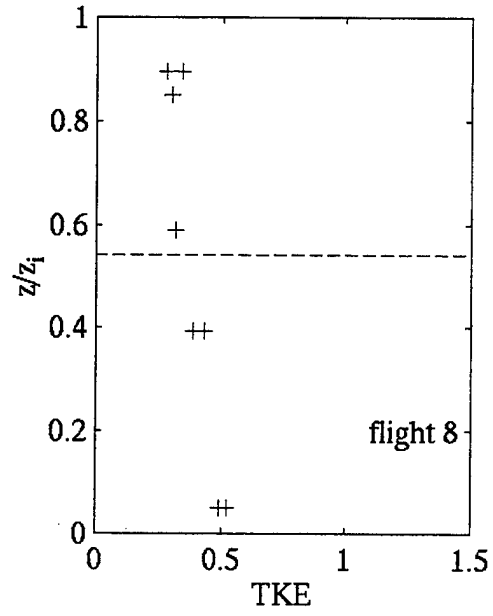
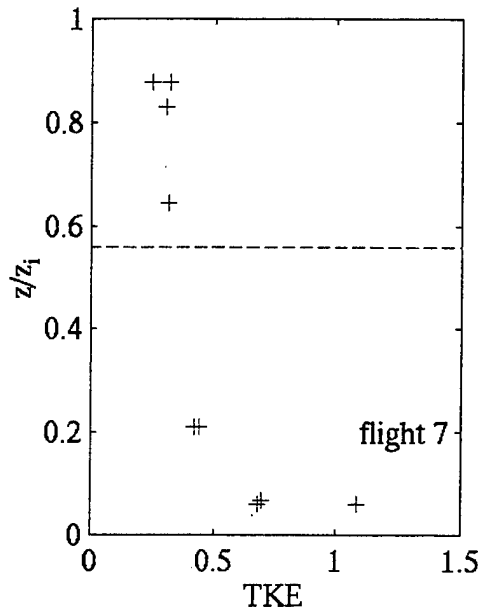


Figure 4, Continued.

4) have the largest BL mean TKE. This is particularly true in the nocturnal case of flight 3 which also has the largest buoyancy forcing from the cloud mixed layer compared to all the other daytime flights. In the decoupled cases, the TKE profiles show rather weak turbulence in the cloud mixed layer compared to the surface-based layer. However, the convective velocity scale ( $w^*c$ ), or the cloud-top buoyancy forcing, is not particularly small relative to the well-mixed cases (except for flight 3). These observations appear to suggest that the surface forcing is crucial in maintaining turbulence in the upper BL. Decoupling thus not only cuts off the moisture supply to the cloud layer, but also cuts off the TKE transport from the surface-based layer to the cloud-mixed layer. Further in-depth comparison with more well-mixed BLs is necessary to consolidate this finding.

Comparison of columns 2 and 3 in Table 2 show the relative importance of the buoyancy and shear, respectively, in generating turbulence. The near-surface buoyancy-generated turbulence is calculated as  $\frac{g}{\theta} \overline{w'\theta'}$  and the near-surface shear-generated turbulence is calculated as  $-(\overline{w'u'} \frac{\partial \overline{U}}{\partial z} + \overline{w'v'} \frac{\partial \overline{V}}{\partial z})$ . Both are terms of the TKE budget equation (Stull 1988).

We found substantial variations from flight to flight in the surface forcing. The wind shear and the turbulence generated are significantly stronger in flights 6 and 8 compared to other flights, and are weakest in flight 2. The buoyancy-generated turbulence varies from  $-2.34 \text{ m}^2\text{s}^{-3}$  to

5.10  $\text{m}^2\text{s}^{-3}$ . The strong variation of sea surface temperature in the coastal upwelling region is the main reason for this large variation (e.g., Rogers et al. 1998). In all flights except flight 2, the shear-generated turbulence is much larger than the buoyancy-generated turbulence, which is consistent with eastern boundary near-surface conditions being close to neutral.

THIS PAGE INTENTIONALLY LEFT BLANK

### III. GEOMETRIC PROPERTIES OF CONVECTIVE EVENTS

#### A. CONDITIONAL SAMPLING METHOD

This study uses a conditional sampling method to identify the turbulent updrafts and downdrafts responsible for vertical transport within the mixed layer and entrainment at the BL top. Nicholls (1989), Lenschow and Stephens (1980), Khalsa and Greenhut (1985), Khalsa (1993), and Wang (1993) use a similar method for both the clear and cloudy BL. Conditional sampling is a technique in which a time series is selectively sampled according to specific criteria. The criteria are applied to a selected indicator variable. Vertical velocity is commonly chosen as the indicator variable, in which case updrafts and downdrafts within the BL are identified. If water vapor is used as an event indicator variable, as in Lenschow and Stephens (1980), the selected event will be moist/dry events. The event indicator variable also defines the boundaries of each event so that the geometric characteristics of the events can be identified. The criteria for event selection therefore include both the magnitude of the indicator variable and the size of the event. Khalsa (1993) describe the technique of conditional sampling in detail.

Wang (1993) tested different thresholds of vertical velocity and event width in selecting appropriate criteria for the conditional sampling of the FIRE data. She found that the results using the thresholds from Nicholls (1989) were very similar to those using thresholds based on visual inspection of the FIRE data. This suggested that the Nicholls criteria captured most of the convective elements

significant to turbulent transport in the FIRE region. Based on these results, this study will use conditional sampling criteria similar to Nicholls (1989).

The conditional sampling scheme used in this study is described briefly here. The vertical velocity data is band-pass filtered prior to the application of the criteria to eliminate variations at scales smaller than 40 m and larger than 3 km. This prevents selection of small spurious events while at the same time preventing larger events from being discounted due to small breaks. The boundaries of an event are determined by the zero-crossing point of the filtered vertical velocity. Based on the Nicholls criteria, threshold vertical velocity is  $w^*/2$ ,  $w^*$  being the cloud convective velocity scale, and the minimum length of the event is  $z_i/20$ ,  $z_i$  being the BL depth. Tables 1 and 2 show that the BL height from all flights are similar, while three of the flights had a  $w^*$  between 0.3 and 0.4  $\text{ms}^{-1}$ . For simplicity, the length criterion is set at a constant 40 m, and the vertical velocity criterion is set at a constant 0.2  $\text{ms}^{-1}$  for all flights. The event selected will be tagged by a new time series called the indicator function, where the updraft, downdraft and background environment are represented by 1, -1, and 0, respectively. Figure 5 shows an example of the identified events.

This study will analyze the updraft and downdraft geometric characteristics and will present the results in the next section. Chapter IV will investigate the leg-averaged properties of thermodynamic and microphysical quantities within the updrafts and downdrafts. The objective is to understand the convective activity in the stratocumulus-topped BL, and specifically the role of



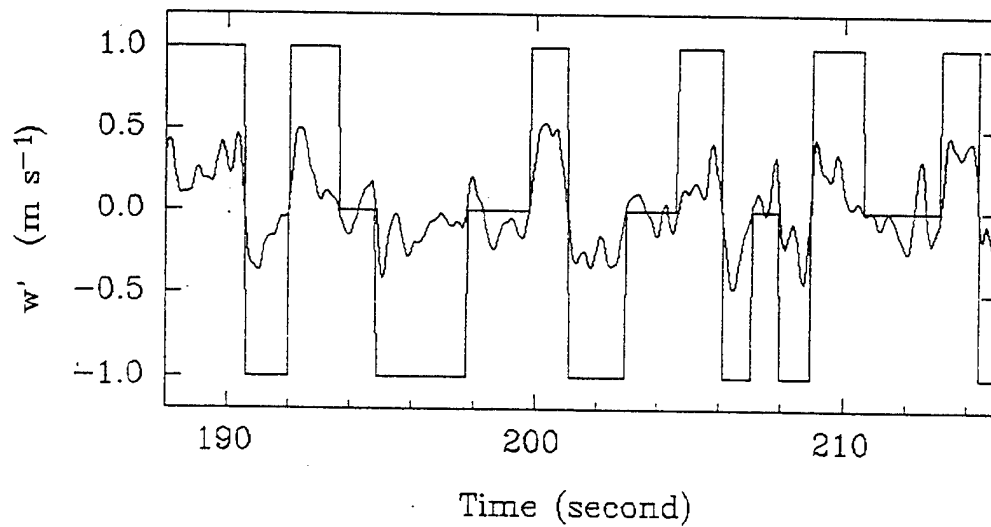


**Figure 5.** Examples of the Conditionally Sampled Updrafts and Downdrafts Identified Using the Identification Functions of 1, -1, and 0 for Updrafts, Downdrafts, and Environment, Respectively. The curved solid line is the band-pass filtered vertical velocity based on which the events were identified. (from Wang 1993).

convective updrafts and downdrafts in turbulence transport and in the microphysical processes.

## B. GEOMETRIC CHARACTERISTICS OF EVENTS

The following section analyzes the average sizes of and fractional coverage by the updrafts and downdrafts within the BL. Results from the conditional sampling method on the number of events occurring in each horizontal flight leg and the average size of each event will allow determination of the geometric characteristics. The mean event size  $\langle d \rangle$  (the average horizontal width of an updraft or downdraft) within a defined flight leg is calculated as (Wang 1993):

$$\langle d \rangle_{u,d} = \frac{\sum_i d_{u,d}}{n_{u,d}}, \quad (3)$$

where  $d$  is the width of each event,  $n$  is the total number of events sampled in the leg, and  $u$  and  $d$  denote updrafts and downdrafts, respectively. The event number frequency  $N$  (the number of events per unit horizontal length) is calculated as (Wang 1993):

$$N_{u,d} = \frac{n_{u,d}}{L}, \quad (4)$$

where  $L$  is the length of the horizontal leg that provided the measurements for conditional sampling. The product of  $\langle d \rangle$  and  $N$  thus defines the proportion of the leg occupied by updrafts or downdrafts, and also defines the fractional area occupied by the events when the events are randomly distributed in space, which is a reasonable assumption for the stratocumulus-topped BL (Nicholls 1989).

Figures 6 through 8 show the vertical profiles of the mean event size, number frequency, and fractional area occupied by the events plotted as a function of height scaled to the BL height ( $z/z_i$ ). The event size is scaled by the BL height. The number frequency is presented as  $N \cdot z_i$  to indicate the number of events on a horizontal distance equivalent to the BL height. Unfortunately, the scaling by  $z_i$  has little significance in this study because the BL heights of all FIRE flights are similar.

In general, it is seen that the mean event sizes (Figure 6) are between 10 and 30 percent of  $z_i$ , or about 200-300 m in the cases of FIRE. In all cases (except for Flight 9), the convective event size in the upper BL is about 0.2 to 0.3 of the BL height, while the near-surface event size is between  $0.10z_i$  and  $0.15z_i$ . The vertical variation of the event size appears to behave differently in the three well-mixed cases (flights 3, 4, and 6) compared to the three clearly decoupled cases (flights 2, 7, and 8). In the well-mixed cases, the event size increases with height rapidly (below  $0.2z_i$ ) from the small near-surface value to a constant mixed layer value of  $0.2z_i$  to  $0.3z_i$ . In the decoupled cases, however, the event sizes hold constant at the near-surface value up to  $0.4z_i$ . It is likely that the entire surface-based layer has a constant value of  $0.10z_i$  to  $0.15z_i$ . The results suggest that decoupling indeed suppresses the growth of the convective events. However, because of the insignificance of the  $z_i$  scaling, the fact that all events in the surface-based layer are between  $0.10z_i$  and  $0.15z_i$  does not necessarily mean that the event size in the surface-based layer scales well with the BL height in the decoupled cases.

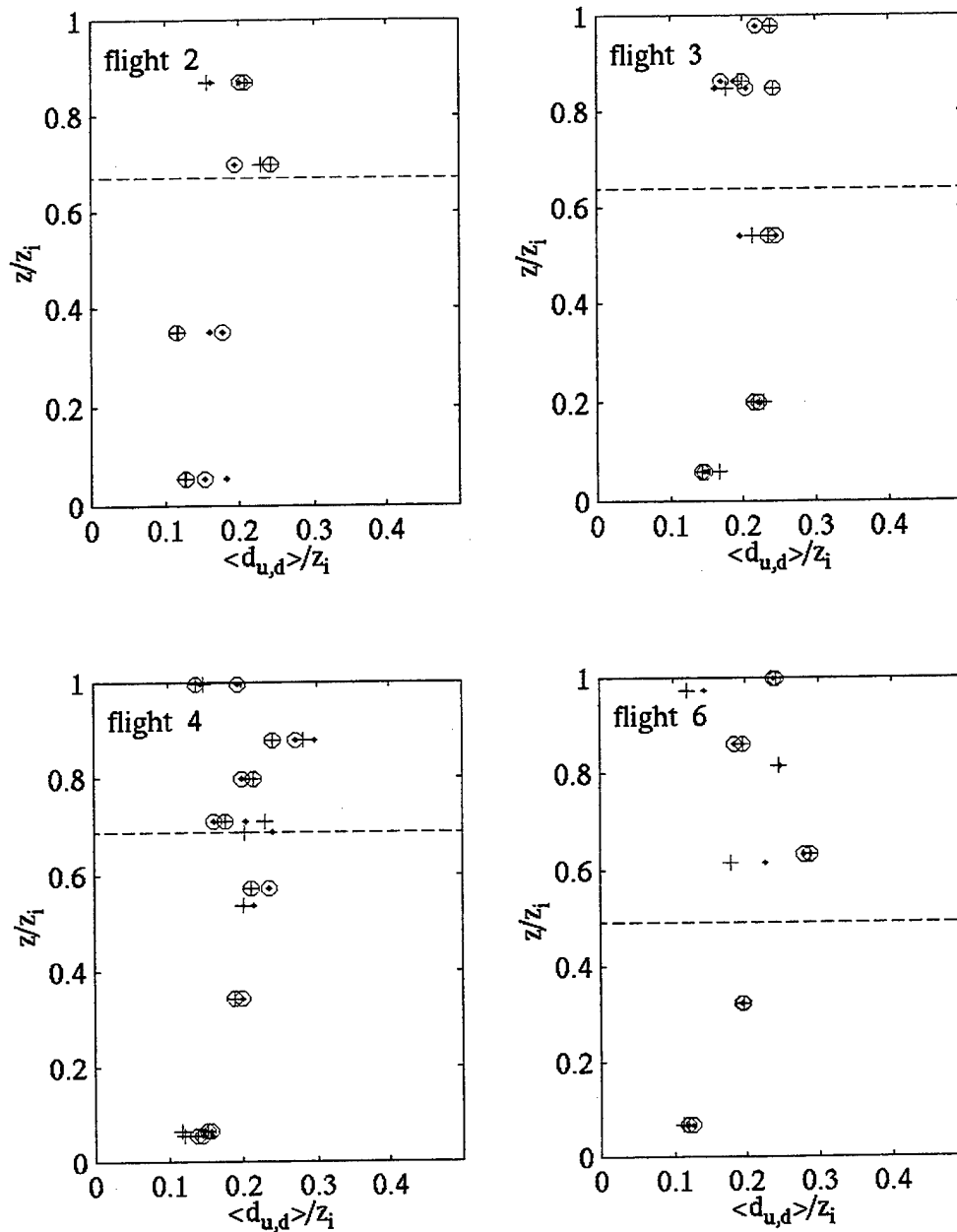


**Figure 6.** Mean Event Sizes for Updrafts (+) and Downdrafts (·), Scaled by the BL Depth, for the Horizontal Turbulence Legs of all Seven Flights. Circled or uncircled symbols at the same level go together as the updraft/downdraft pair for a given leg. The dotted line shows the average height of the cloud base.

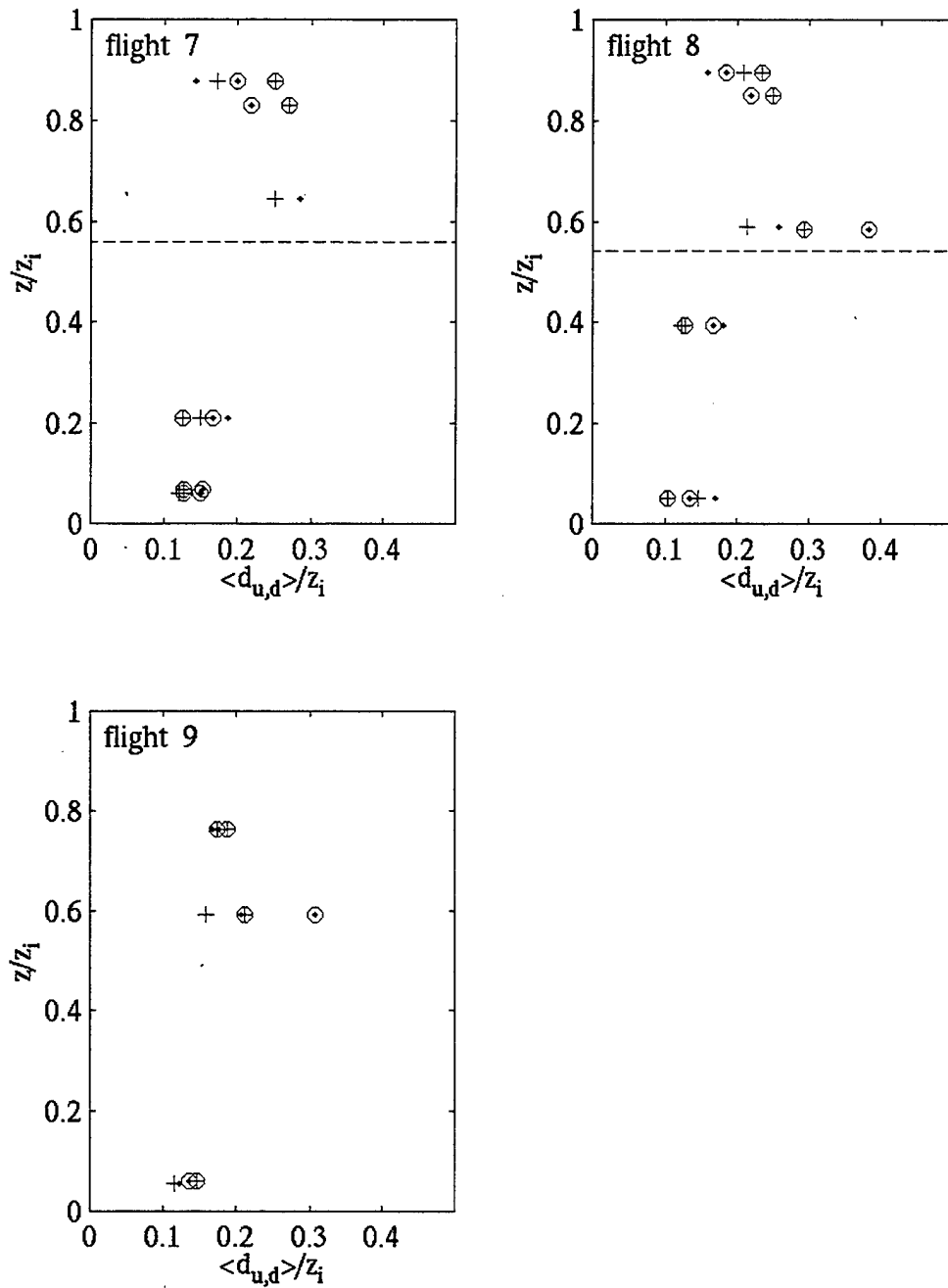
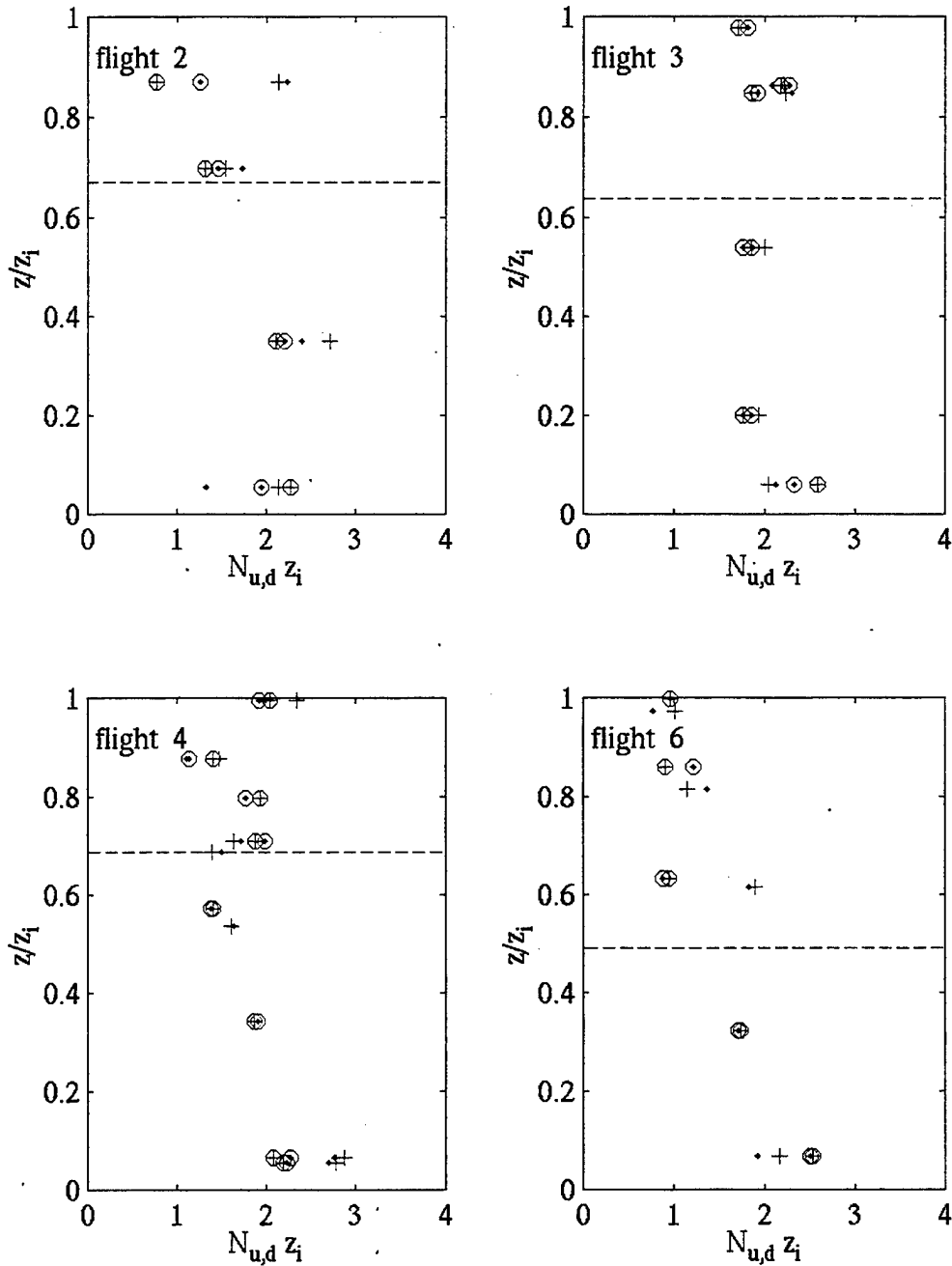


Figure 6, Continued.

The number frequency of events (Figure 7) is smaller in the upper BL than in the near-surface layer in all cases. Compared to the trend of vertical variation of the event size, this decrease seems to correlate with the increase of the event size. Therefore, the decrease in number of events is a result of the increase in event size. The strongly well-mixed case (flight 3) is the only case that does not show sizable decrease in number of convective events with height. This appears to agree with the findings in Young (1988) for the well-mixed clear convective BL.

In flights 2, 4, 7, and 8, the downdrafts are larger in size and occupy a larger fractional length (Figure 8) than the updrafts in the surface-based layer. In chapter II it was noted that these flights had large surface buoyancy fluxes compared to the in-cloud buoyancy fluxes. It is likely that the larger surface buoyancy flux is generating concentrated updraft plumes in the near surface layer. Randall (1980) and Wang (1993) suggest that the larger size of downdrafts implies positive vertical velocity skewness (i.e., the updrafts are more vigorous than the downdrafts). In flight 8, vertically well-developed cumulus existed below, and often extended up into the main stratocumulus deck during this flight. This development would tend to concentrate relatively strong updrafts into a smaller area in the surface layer, explaining the dominance of the area by the downdrafts. The opposite is true for the flights with small positive (flights 3 and 9) or negative (flight 6) surface buoyancy fluxes. Here the updrafts occupy slightly more area than the downdrafts. In contrast, because the in-cloud buoyancy flux is large for flight 3, the updrafts occupy a larger fractional length than the downdrafts near the top of the BL.



**Figure 7.** Same as in Figure 6, Except for Event Frequency. The product  $N \cdot z_1$  describes the number of events in a horizontal length equivalent to the BL depth.

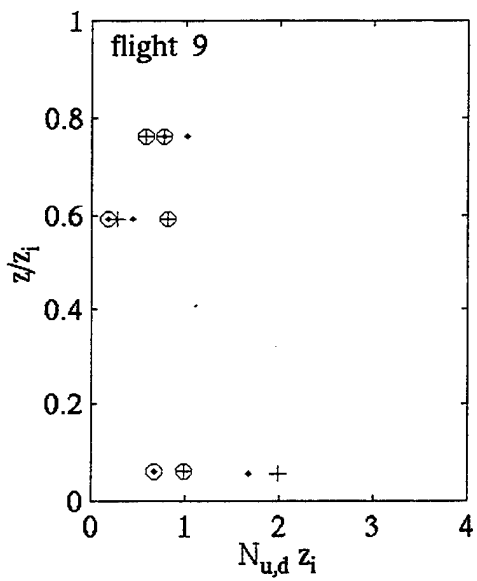
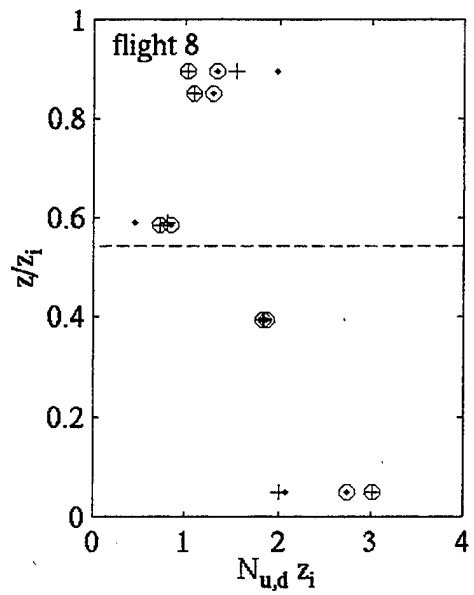
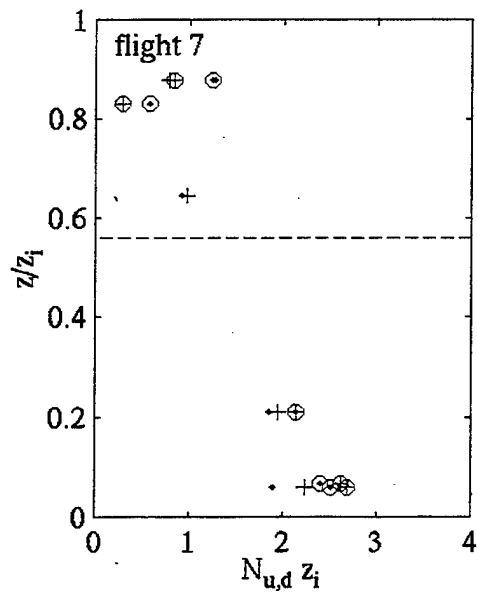
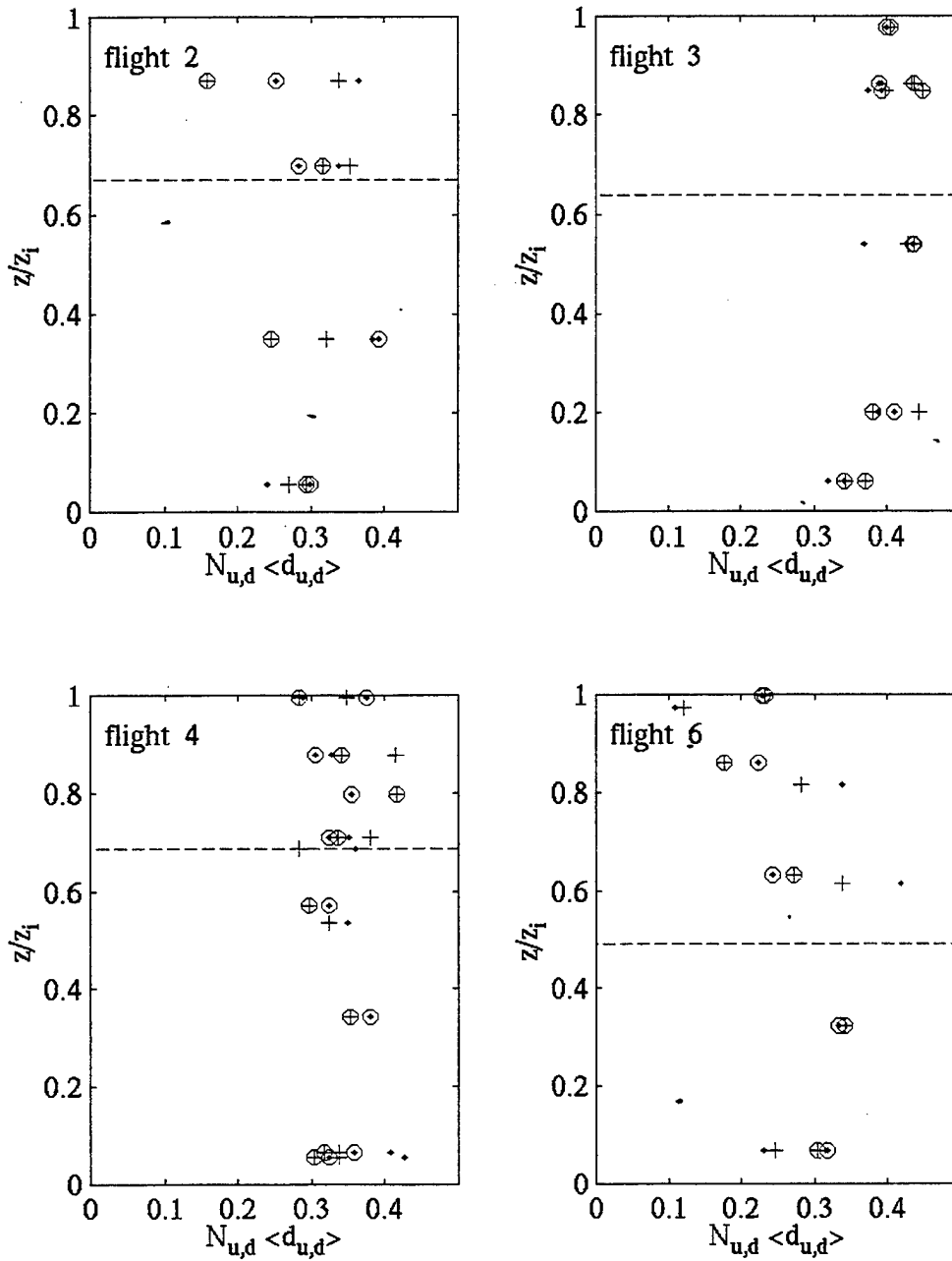


Figure 7, Continued.





**Figure 8.** Same as in figure 6, Except for Fractional Length Covered by Updrafts and Downdrafts.

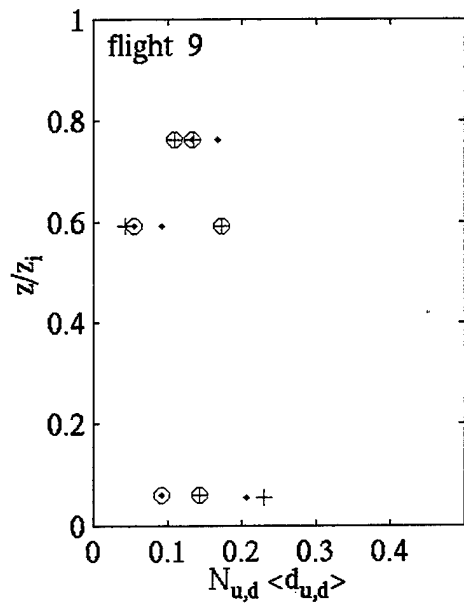
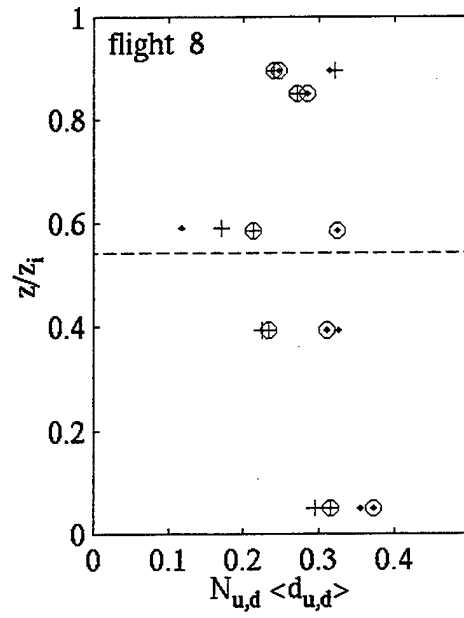
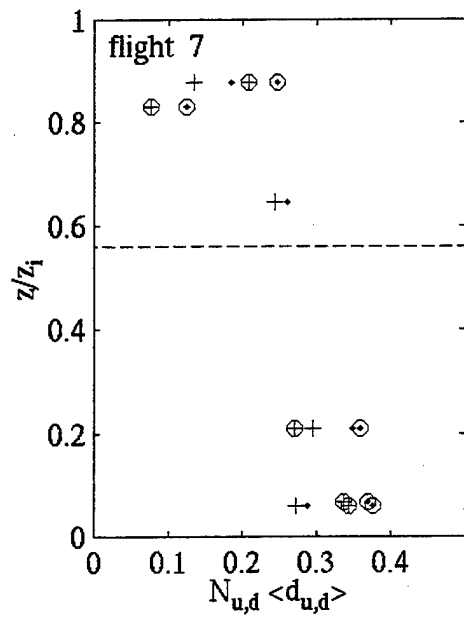


Figure 8, Continued.

The total fractional length covered by convective events varies significantly between the different flights and between different levels in the BL within each flight. The two clearly well-mixed cases, flights 3 and 4, have the largest fractional length coverage by convective events, between 0.6 and 0.8. Young (1988) reported that the fractional area coverage by thermals in the clear convective BL is largest near the surface and near the top of the BL, and smallest near the middle of the BL. He also states that the fractional length coverage is less than 0.5 throughout most of the BL, with minimums ranging from 0.36 to 0.43 in the mid-BL. Other studies by Manton (1977), Lenschow and Stephens (1982), and Greenhut and Khalsa (1987) also report smaller values than the ones found here for the FIRE data. In flights 2, 3, and 4, and 6 the fractional length occupied by the updrafts and downdrafts increases with height through the surface-based layer. This trend is also observed by Khalsa and Greenhut (1985). These flights also have the highest fractional length values within the cloud mixed layer. In flights 7, 8, and 9 the fractional length decreases with height in the surface layer, and therefore the highest fractional length values are in the surface layer. Flights 3 and 7 are the extreme cases in each category, where these trends are clearly seen in Figure 8. These trends are related to the strength of turbulence at each level in the BL. Stronger turbulence means that a greater area will be occupied by updrafts and downdrafts. For instance, flight 3 has a large convective vertical velocity in the cloud layer, implying strong cloud layer turbulence, and weak surface layer turbulence (see chapter II, Table 2). The opposite structure is observed in flight 7.

THIS PAGE INTENTIONALLY LEFT BLANK

#### IV. THERMODYNAMIC AND MICROPHYSICAL PROPERTIES OF CONVECTIVE EVENTS

##### A. THERMODYNAMIC PROPERTIES

Figures 9 through 13 show the vertical profiles of several thermodynamic quantities in both the updrafts and downdrafts in the horizontal turbulence legs of the FIRE flights. The vertical velocity and liquid water are averaged over all updraft or downdraft events in the turbulence leg, to obtain an event average. The virtual potential temperature and water vapor content are band-pass filtered to remove the low frequency perturbations, and then averaged over all updraft or downdraft events in the turbulence leg to obtain an average perturbation from the mean.

The mean vertical velocity in both the updrafts and downdrafts for all flights is fairly symmetrical with height in the BL. The vertical variation of the event vertical velocity (Figure 9) is consistent with that of the variance of vertical velocity (not shown). Here the nocturnal case of flight 3 has the strongest convective events as a result of strong radiative and evaporative forcing (Wang and Albrecht 1994).

The virtual potential temperature perturbation (approximately referred to as buoyancy excess) profiles indicate large variability among the flights. Near the surface, the updrafts are in general weak but positively buoyant while the downdrafts are negatively buoyant. These updrafts and downdrafts contribute to the positive TKE buoyancy production indicated in Table 2. The exception is with flight 6, where the sign of buoyancy perturbation is

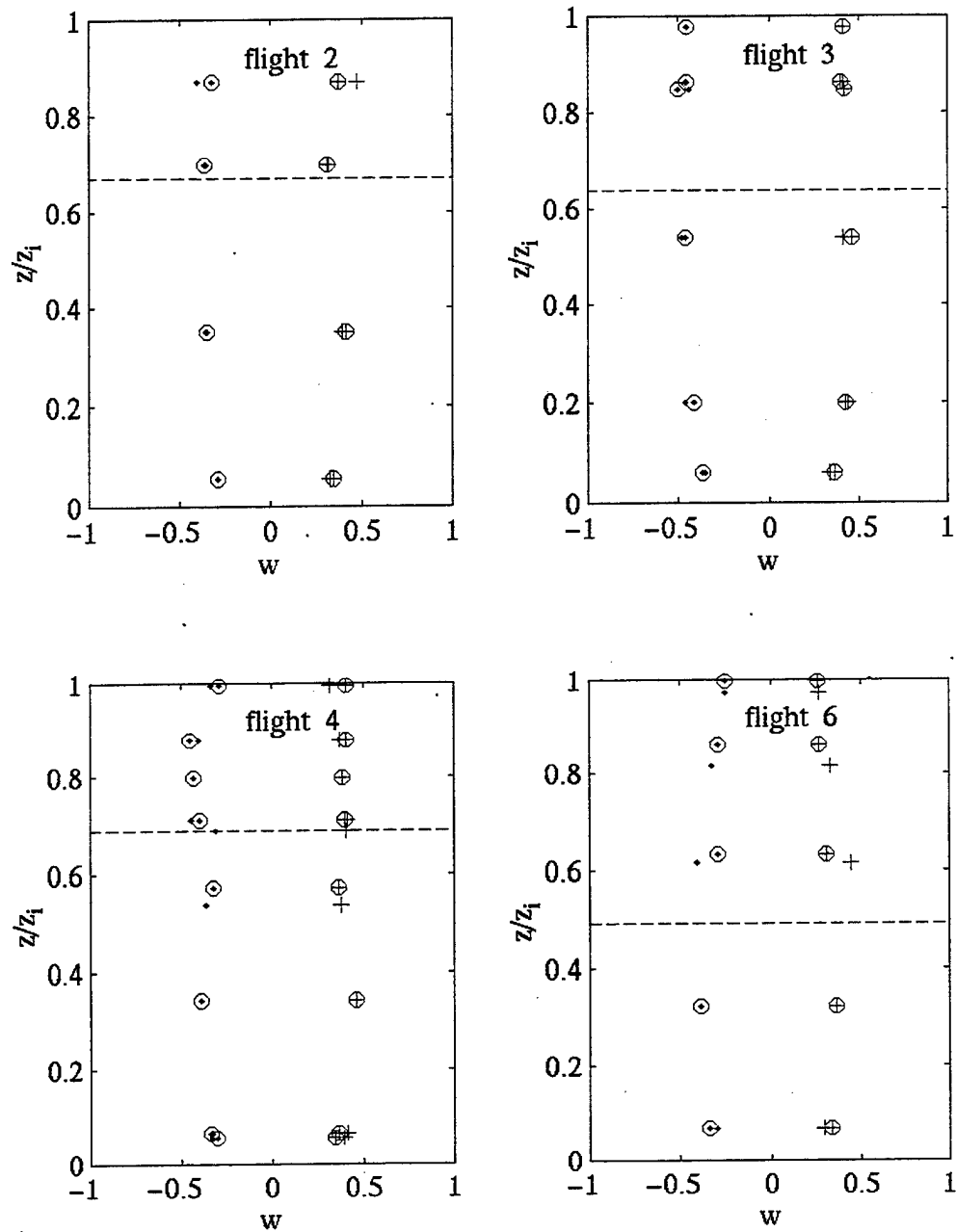


**Figure 9.** Mean Vertical Velocity (in  $\text{m s}^{-1}$ ) for Updrafts (+) and Downdrafts (·), Scaled by the BL Depth, for the Horizontal Turbulence Legs. Circled or uncircled symbols at the same level are the updraft/downdraft pair for a given leg. The dotted line shows the average height of the cloud base.

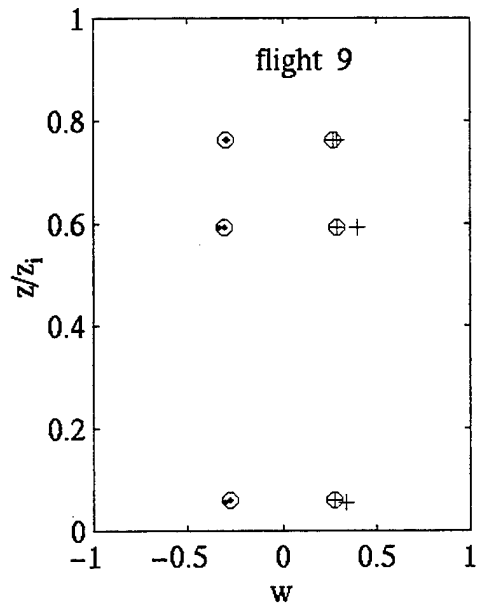
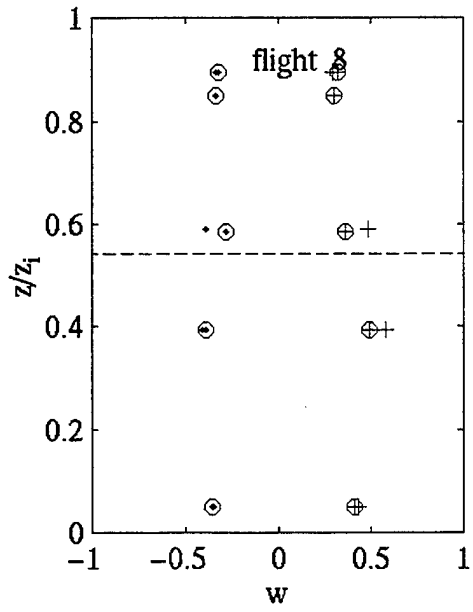
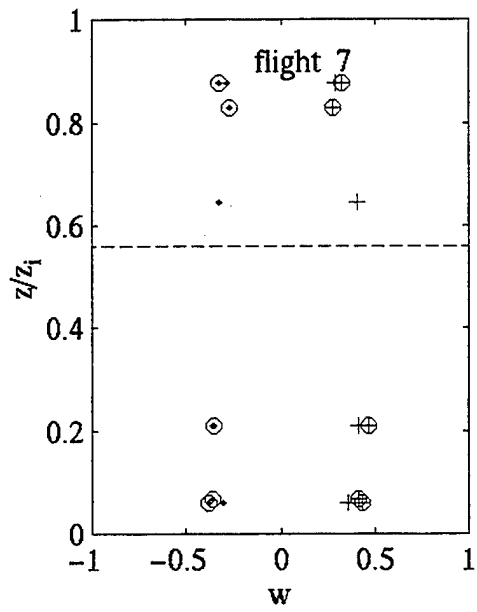


Figure 9, Continued.

completely reversed in correspondence with the negative surface buoyancy flux (Table 2). Figure 10 shows that the cool updrafts can be identified up to  $0.35z_1$ . In the upper BL, signatures of the cool downdrafts and warm updrafts are clear in cases of sizable in-cloud buoyancy flux, such as in flight 3, and recognizable in some flights with weak in-cloud buoyancy forcing (e.g., flights 2, 6, and 8). More complications are observed here especially near the cloud top. In flight 7, however, the downdrafts appear to be warmer compared to the updrafts in the cloud layer. It is noted in Table 2 that turbulence in this flight is largely generated by surface buoyancy flux and wind shear, while the in-cloud generation of TKE is very limited. There is thus no coherence between the vertical motion and the buoyancy excess.

It is known that both radiative cooling and evaporative cooling from entrainment mixing may result in cool downdrafts. The presence of evaporative cooling is identified by the so-called buoyancy reversal criterion (Siems et al. (1990)):

$$\Delta\theta_e < k \frac{L}{C_p} \Delta q, \quad (5)$$

Here,  $\Delta$  denotes the jump across the inversion,  $L$  and  $C_p$  are the latent heat of water phase change and specific heat capacity of dry air, respectively,  $\theta_e$  is the equivalent potential temperature and  $q_t$  is the total water. For typical BL conditions,  $k$  has a value of 0.23. Average inversion jump conditions for the FIRE flights calculated in McDowell (1999) are used in Equation 5. It is found that (5) is satisfied for all seven flights in this study, suggesting



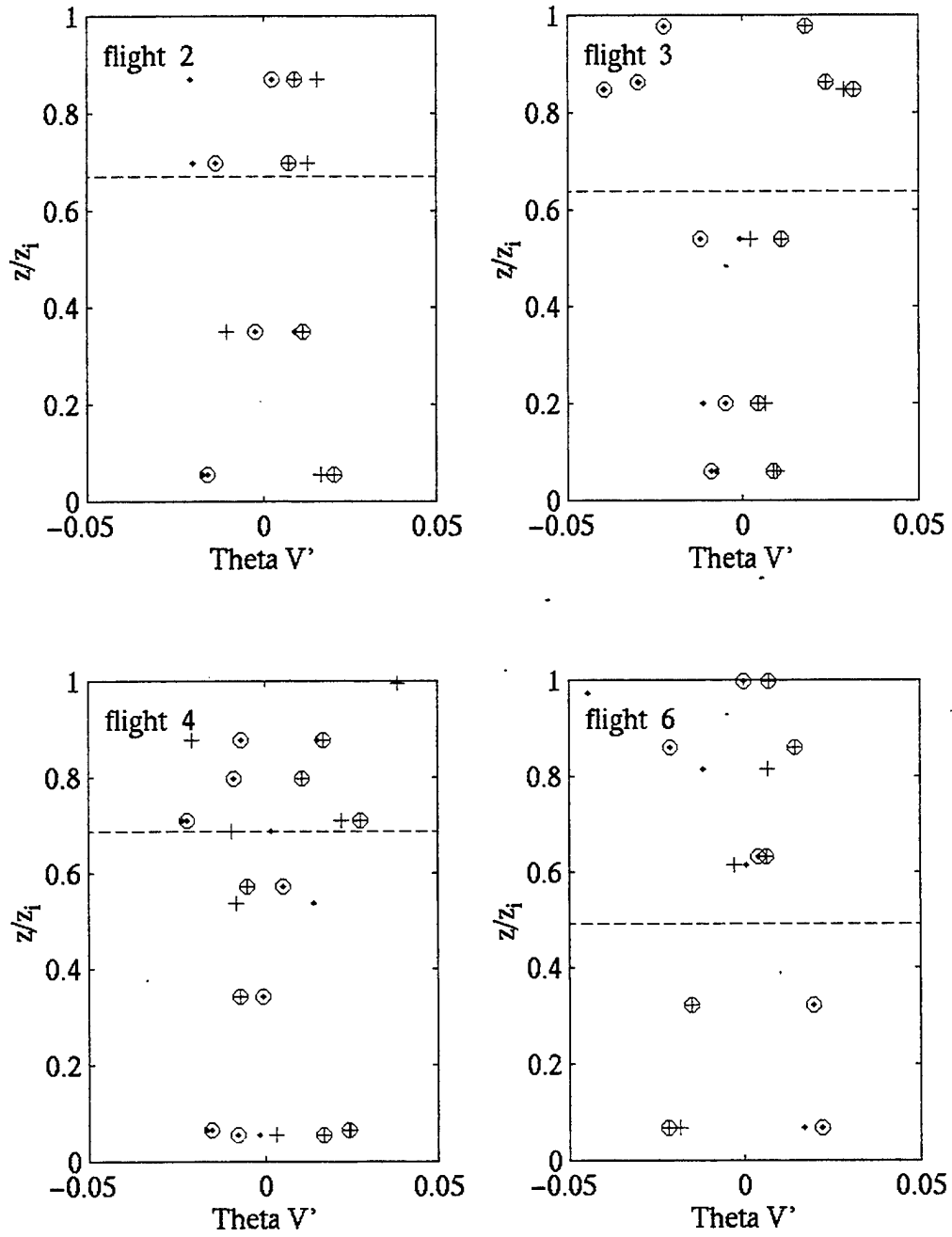


**Figure 10.** Same as Figure 9, Except for Mean Perturbations of Virtual Potential Temperature (in K).

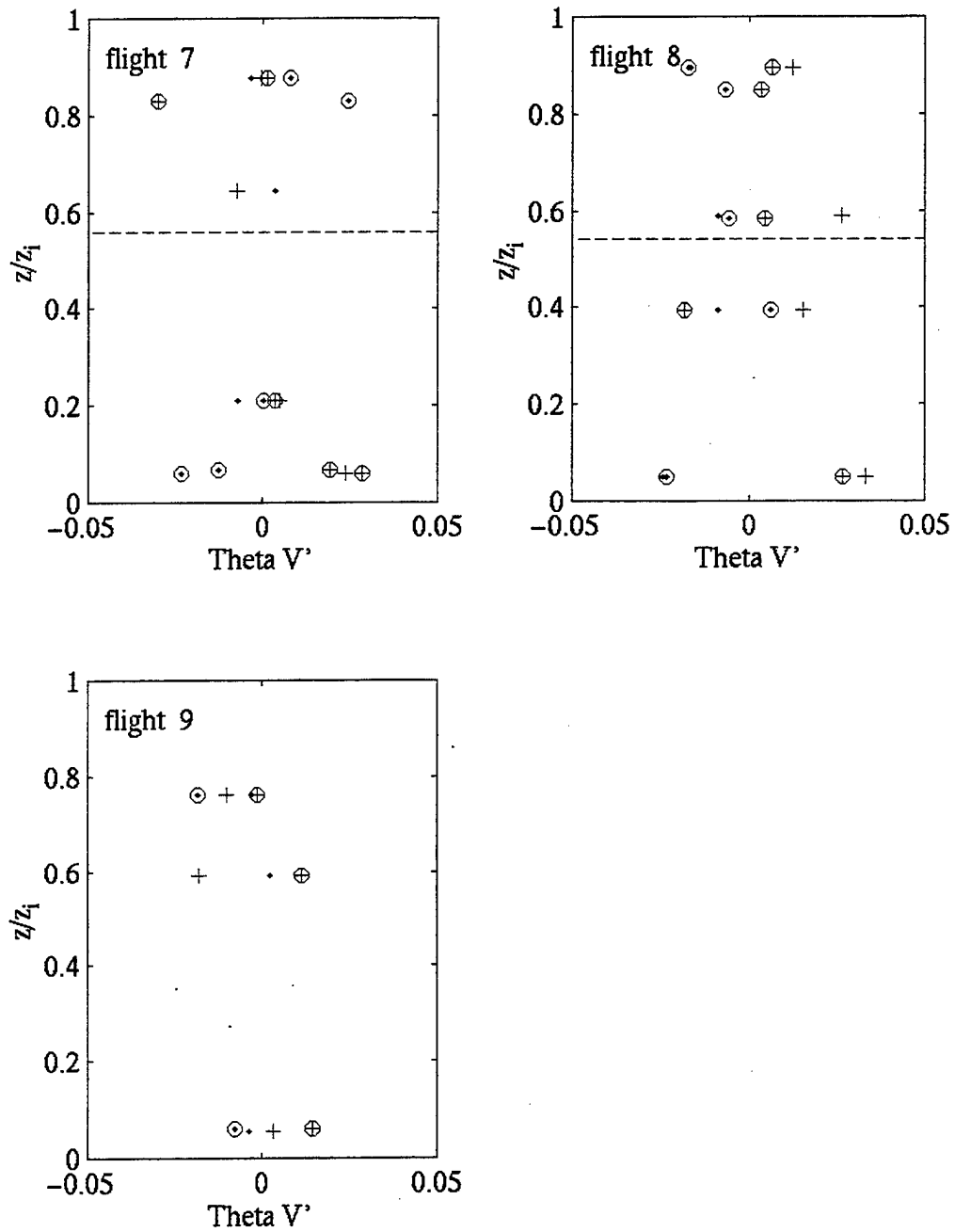
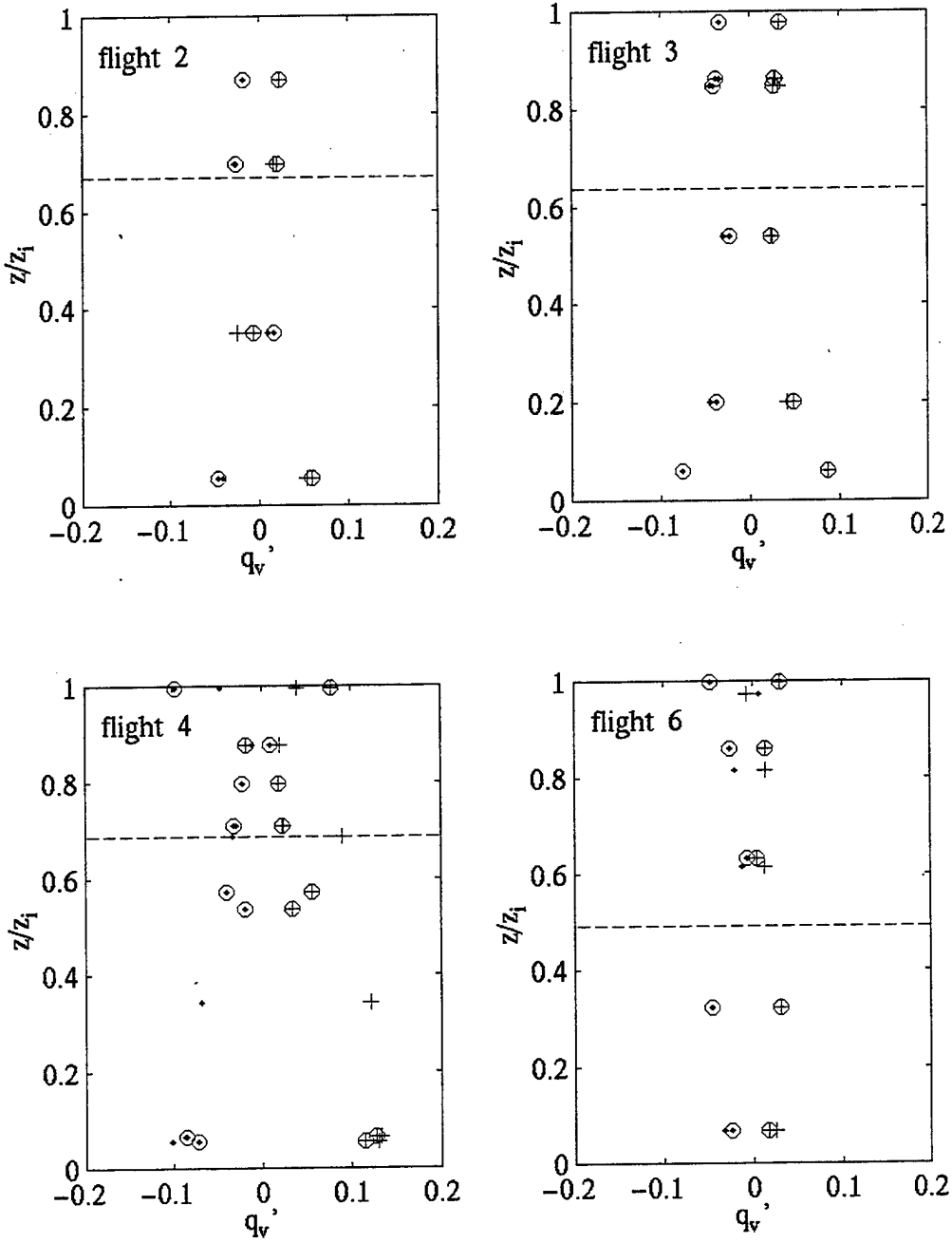


Figure 10, Continued.

that evaporative cooling plays a role in the cool downdrafts in the upper BL in Figure 10.

In all cases, the difference in buoyancy excess in the middle of the BL is very small and may not be significant. Buoyancy production in this region is in general the weakest, and sometimes may be negative (not shown).

A somewhat consistent trend is seen in the vertical profiles of water vapor perturbation. Figure 11 shows large differences between the positive updraft perturbations and the negative downdraft perturbations near the surface in most flights and also near the cloud top in flights 4 and 6. We observe smaller differences in the cloud mixed layer as the perturbations in updraft and downdraft become smaller in magnitude. Near the surface, large positive water vapor perturbations are observed in the updrafts near the large moisture source of the sea surface, and large negative perturbations are observed in the downdrafts as the descending air parcels become warmer and drier compared to the surrounding environment. Minimum values are generally seen in the cloud mixed layer away from the cloud boundaries. Here, both updrafts and downdrafts are likely saturated, so the small difference between the updraft and downdraft is due to small temperature differences, with the updrafts being slightly warmer. The larger differences near the cloud top are likely the result of entrainment, in which case the downdrafts will contain drier and warmer air from above the inversion. As a result, some of the entrainment mixture may become sub-saturated. Note that in flight 6, the updrafts are cool but moist in the stable near-surface environment.



**Figure 11.** Same as in Figure 9, Except for Mean Water Vapor Perturbation (in  $\text{g kg}^{-1}$ ).

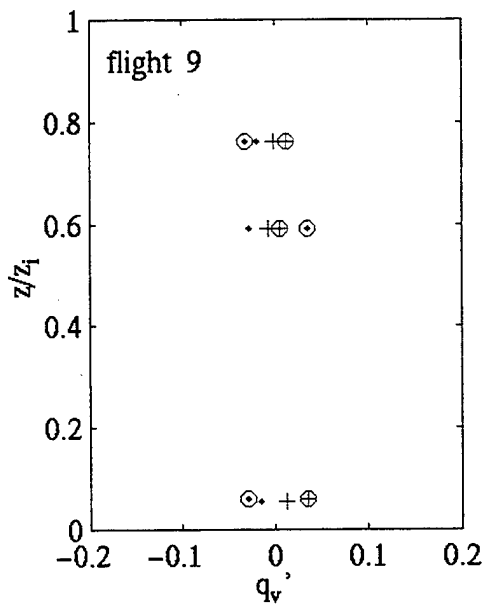
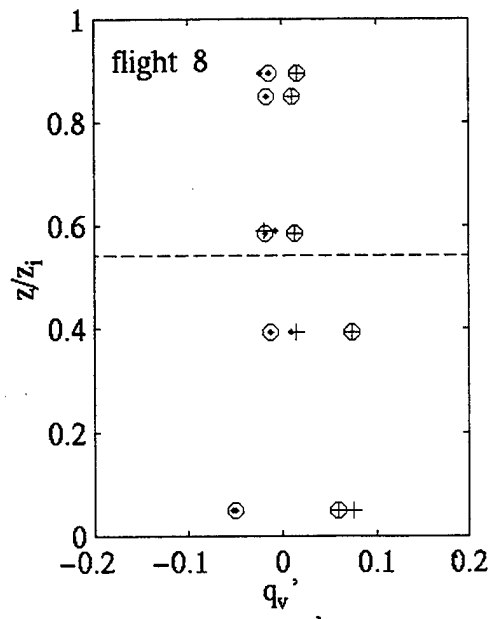
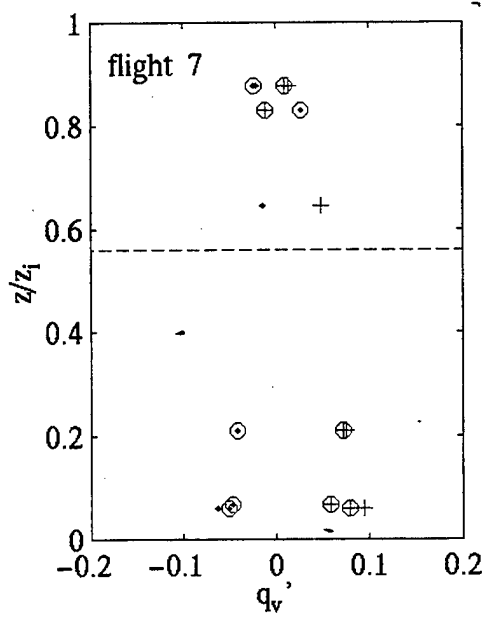
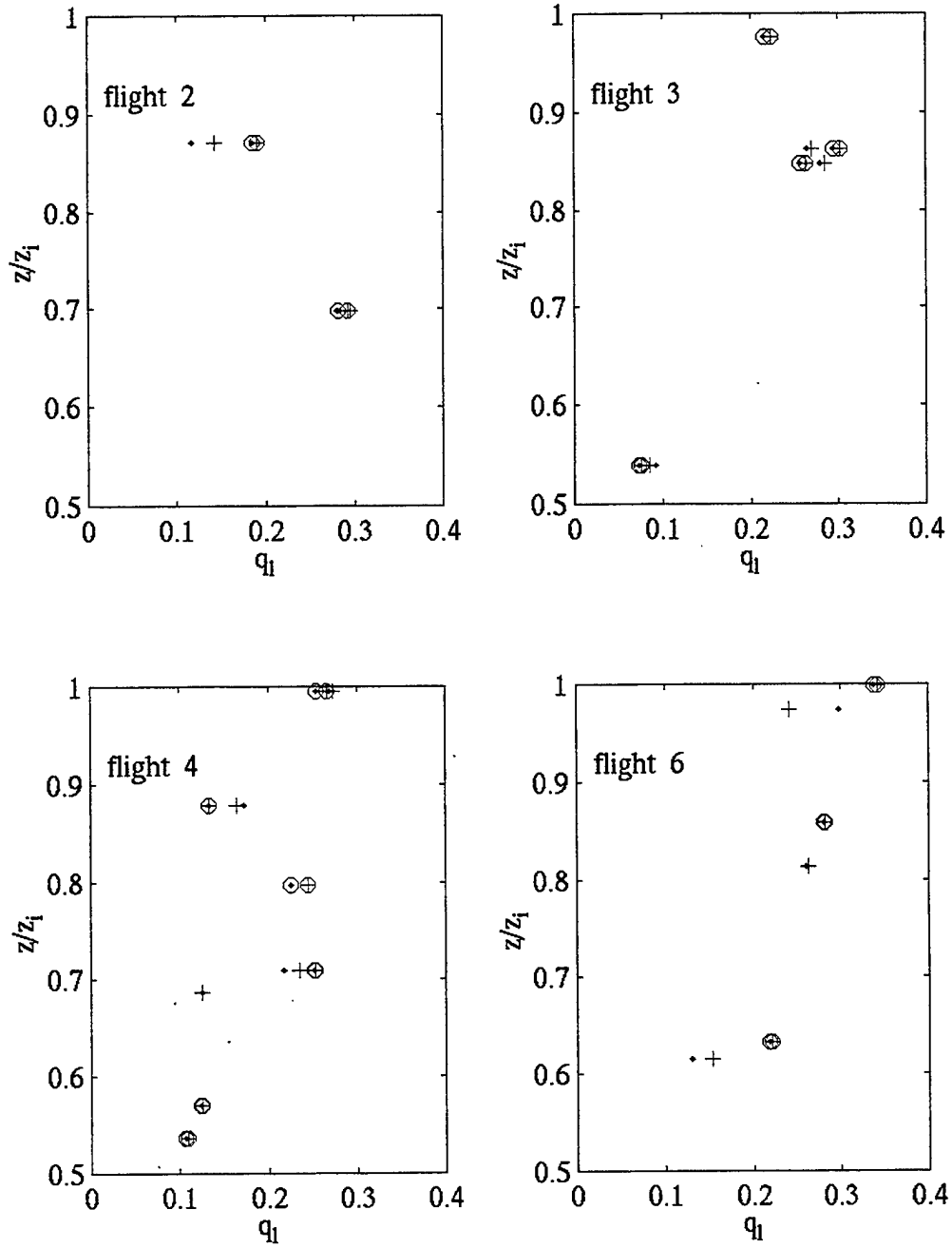


Figure 11, Continued.

Figure 12 shows the vertical profiles of event mean liquid water content for the in-cloud turbulence legs. In all cases except for flight 2, there is a consistent trend of increasing liquid water content with height in both updrafts and downdrafts. The difference between the two types of dynamical events is also noticeable. Figure 13 shows the fractional difference between updraft and downdraft cloud liquid water content. At most levels in all flights the fractional difference between updrafts and downdrafts is positive, suggesting more liquid water content in turbulent updrafts. The difference is, however, small in magnitude, usually less than 5%. Positive differences between updraft and downdraft liquid water content appear to be the largest near the cloud base in most flights. This trend is consistent with the activation and growth of cloud droplets in the updrafts at the cloud base. In flight 3, the maximum difference is near the cloud top. This is likely the reflection of the increased evaporation occurring here as a result of the enhanced turbulent mixing and entrainment (Wang and Albrecht 1994).



**Figure 12.** Same as Figure 9, Except for Mean Liquid Water Content (in  $g\ kg^{-1}$ ).

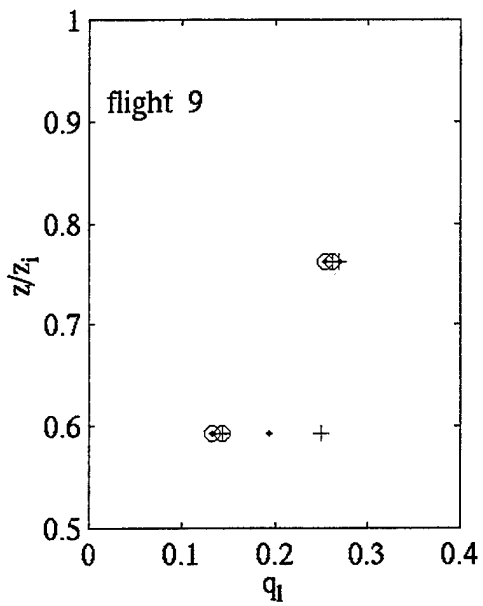
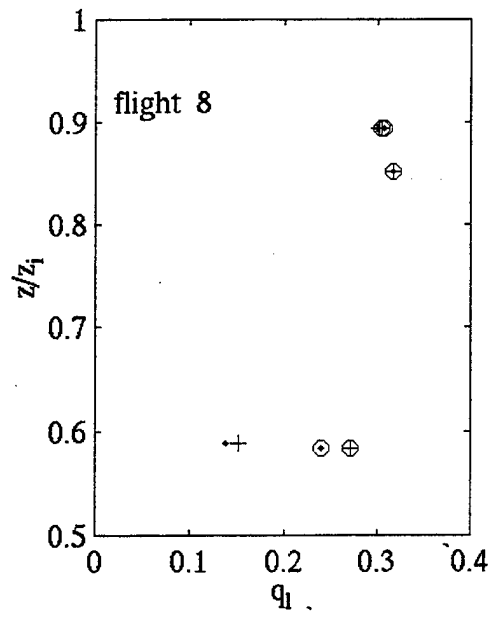
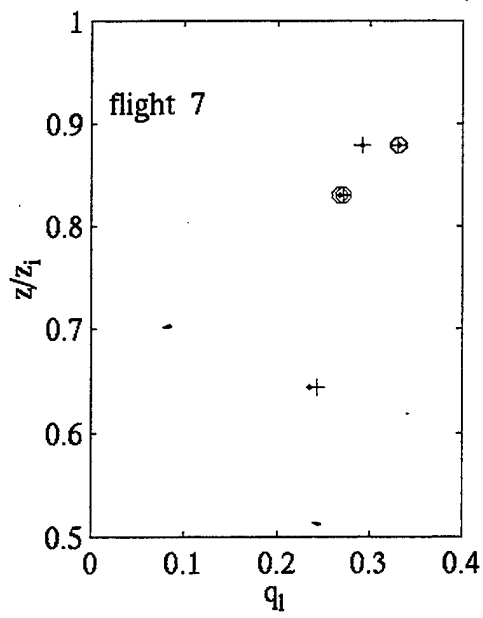
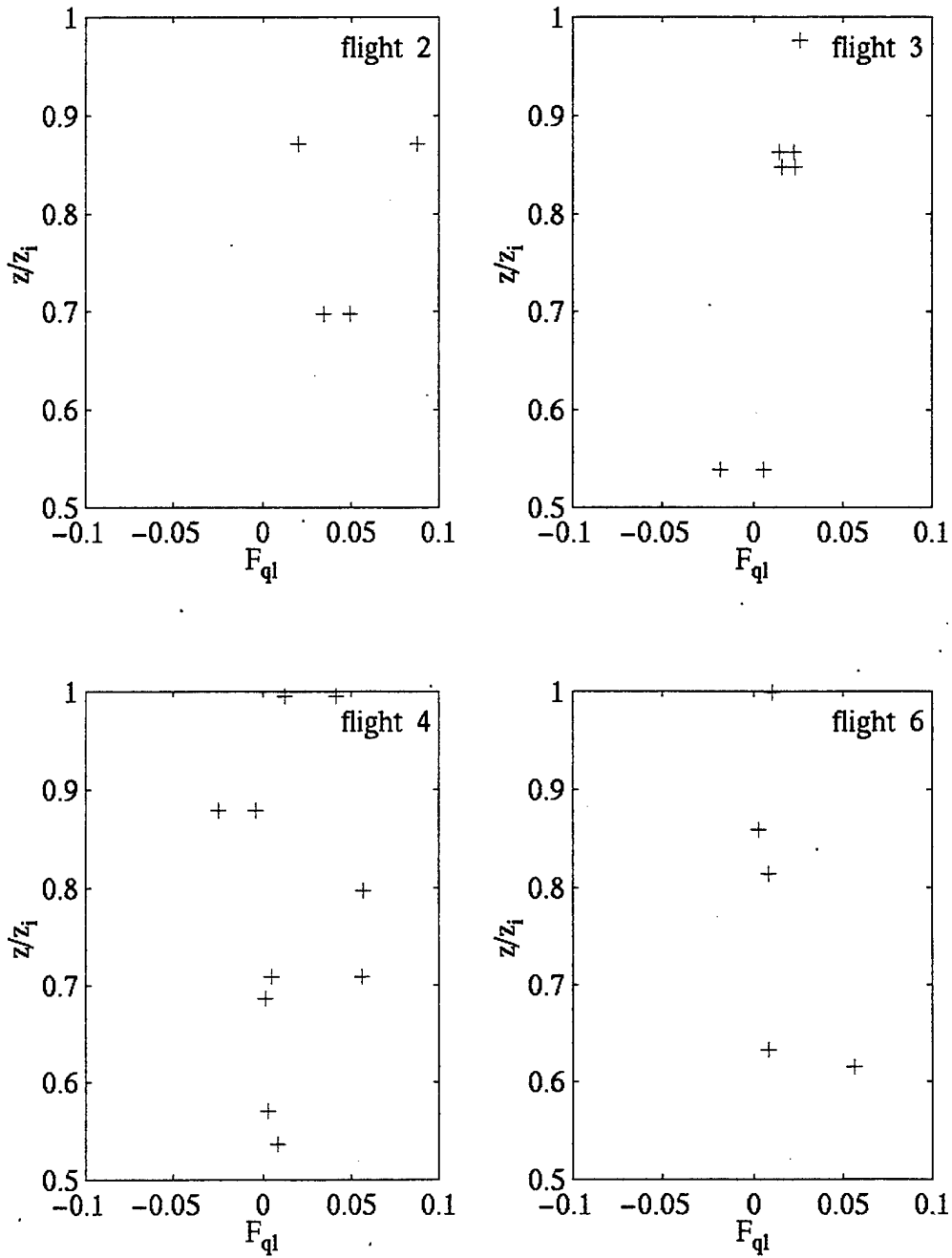


Figure 12, Continued.





**Figure 13.** Fractional difference in Mean Liquid Water Content Between Updrafts and Downdrafts ( $F_{q1}$ ) for the Horizontal Turbulence Legs.  $F_{q1}$  is calculated as:

$$(q_{l_u} - q_{l_d}) / \frac{1}{2}(q_{l_u} + q_{l_d}).$$

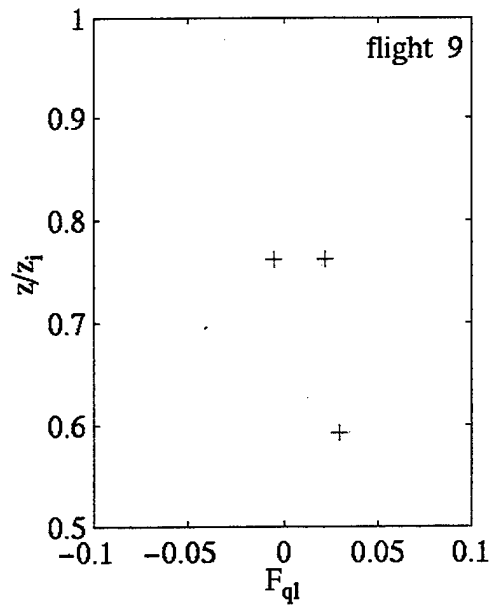
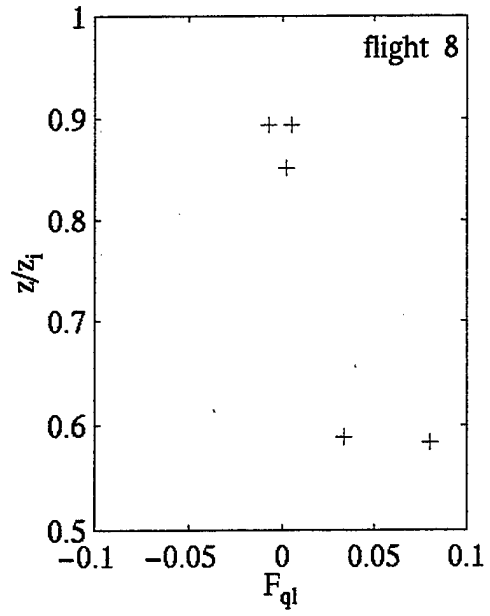
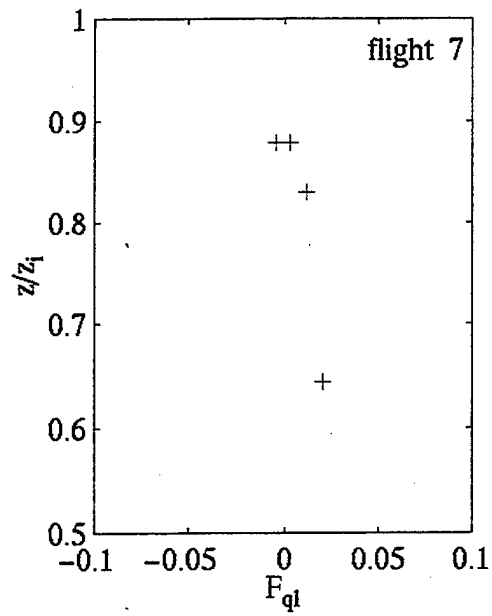


Figure 13, Continued.

## B. MICROPHYSICAL PROPERTIES

### 1. Droplet Concentration and Size

The volume diameter of cloud droplets is calculated as:

$$d_v = \left( \frac{\sum_{k=1}^{15} d_i^3 n_i}{\sum_{k=1}^{15} n_i} \right)^{1/3} \quad (6)$$

where  $d$  is the droplet diameter,  $n$  is the number of droplets, and  $k$  is the size bin of the FSSP. Figure 14 shows the cloud droplet volume diameters for the cloud mixed layers of all flights. In general, the droplet sizes increase with increasing height from the cloud base. This is consistent with results from stratocumulus clouds in other regions (e.g., Nicholls 1984). Near the cloud top, signs of decreased droplet size are observed in some of the flights (flights 2, 3, 4, and 6). It is possible that with more cloud top data for the other flights the same decrease would be seen there as well.

The largest droplet size is found in flight 6, where the maximum droplet diameter near the cloud top is as large as 23  $\mu\text{m}$ . This flight also has the lowest BL depth of all flights (751 m) and a relatively thick cloud layer depth (383 m). The large droplet size is a reflection of the deep cloud layer. Droplet diameters of all other flights average around 15  $\mu\text{m}$  near the cloud top.

The difference in droplet sizes between the updrafts and downdrafts can be clearly identified in Figure 14, where

the dot symbols (downdrafts) are in general to the right of the corresponding plus symbols (updrafts). The fractional difference in volume diameter between the two types of convective events is shown in Figure 15. Although small, this quantity is found to be consistently negative in most cases. This trend indicates that the downdrafts contain the larger droplets originating from higher levels in the cloud, while the updrafts contain droplets still in the growth process. Larger differences are observed near the base and top of cloud, with a minimum difference in the mid cloud range, which is consistent with droplet formation in the updrafts near the cloud base and evaporation due to entrainment in the downdrafts near the cloud top.

The number concentration of droplets in the updrafts is consistently higher than in the downdrafts at all levels within the cloud (Figure 16). Since activation of cloud droplets is occurring in the updrafts and evaporation of droplets is occurring in the downdrafts, these observations are reasonable. Nicholls (1984) showed that the number concentration of droplets in the stratocumulus cloud is fairly constant with height at any given horizontal location in the cloud, which is apparent in a sounding through the entire depth of the cloud (Figure 3). This cannot be observed here since each of the turbulence legs takes place at a different horizontal location within the cloud layer, which causes the apparent scatter in the number concentration between the different legs.

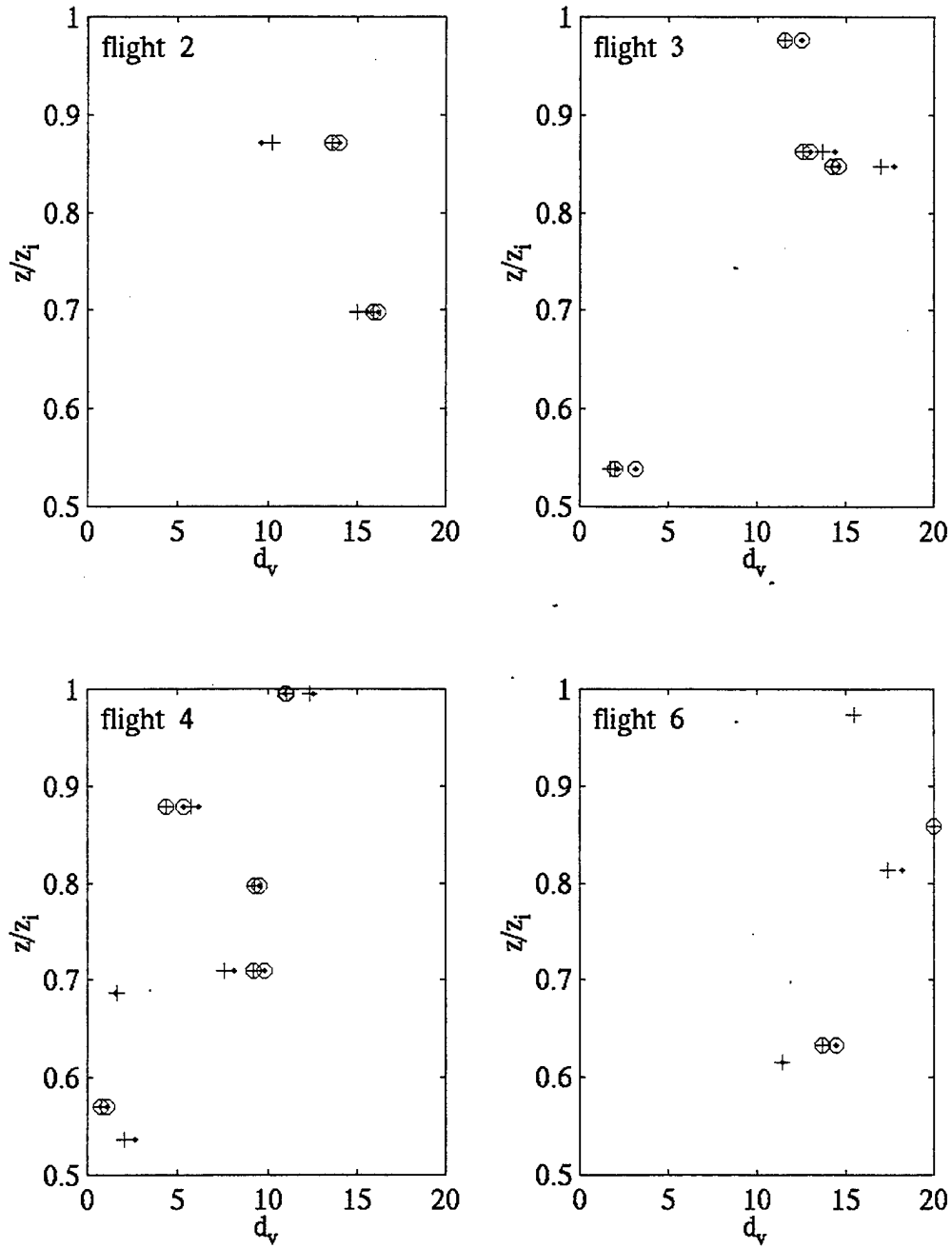


**Figure 14.** Same as in Figure 9, Except for Volume Diameter of Cloud Droplets (in  $\mu\text{m}$ ).

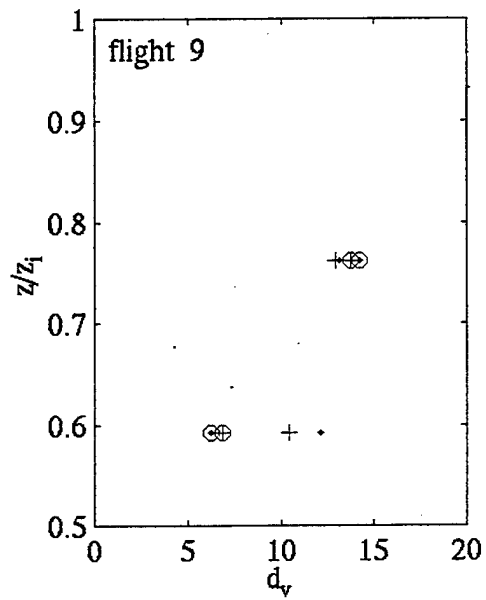
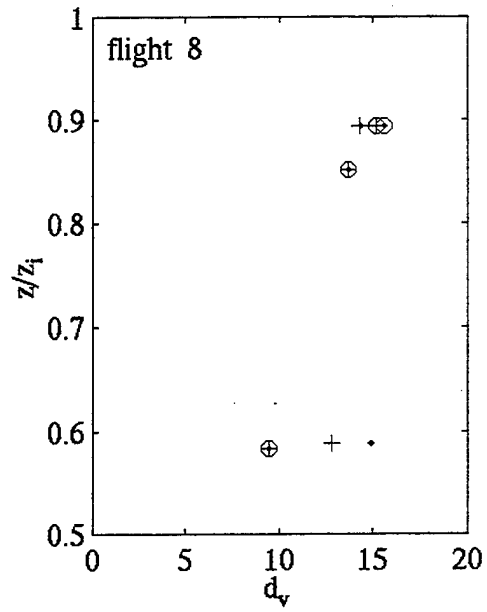
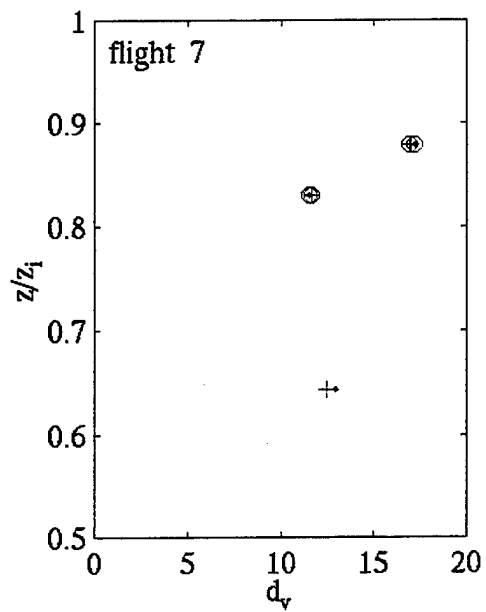
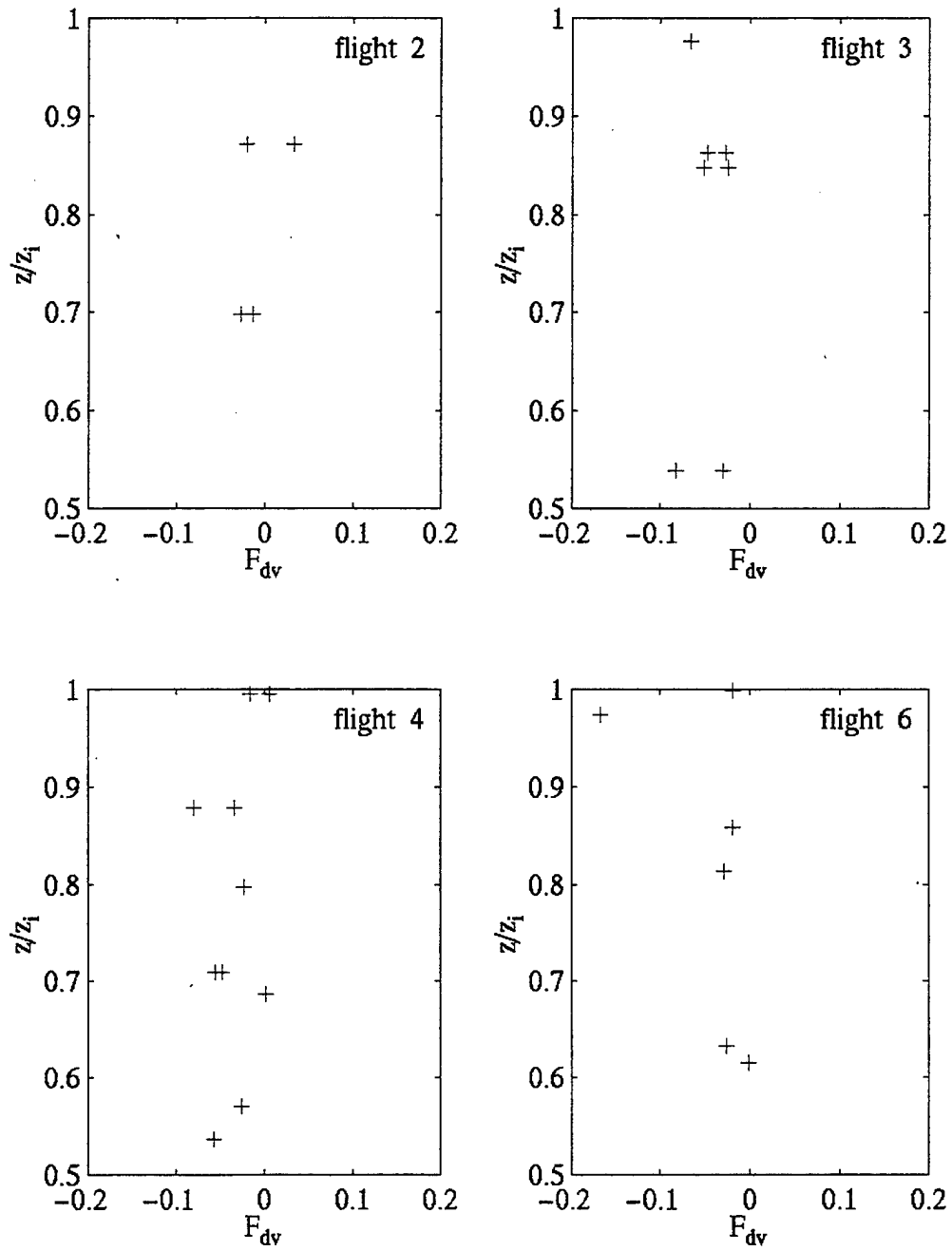


Figure 14, Continued.



**Figure 15.** Same as Figure 13, Except for Fractional Difference for Volume Diameter of Cloud Droplets ( $F_{dv}$ ).  $F_{dv}$  is calculated as:  $(d_{v_u} - d_{v_d}) / \frac{1}{2}(d_{v_u} + d_{v_d})$ .

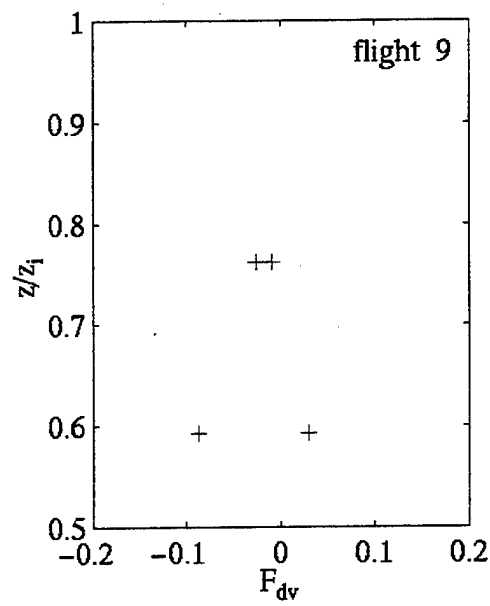
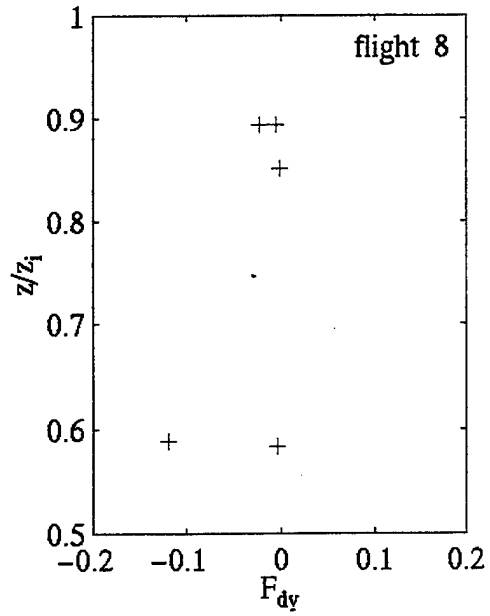
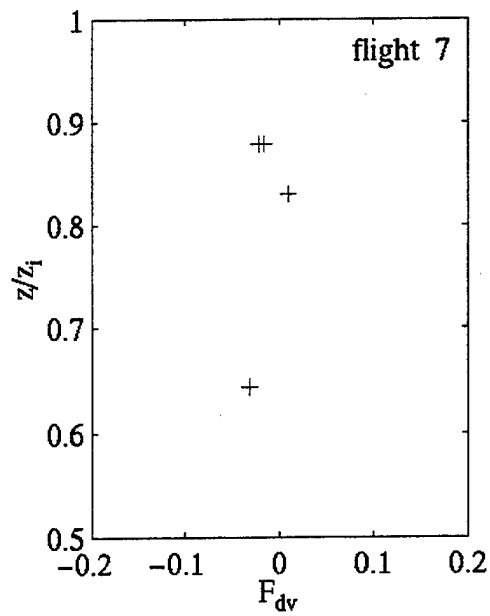
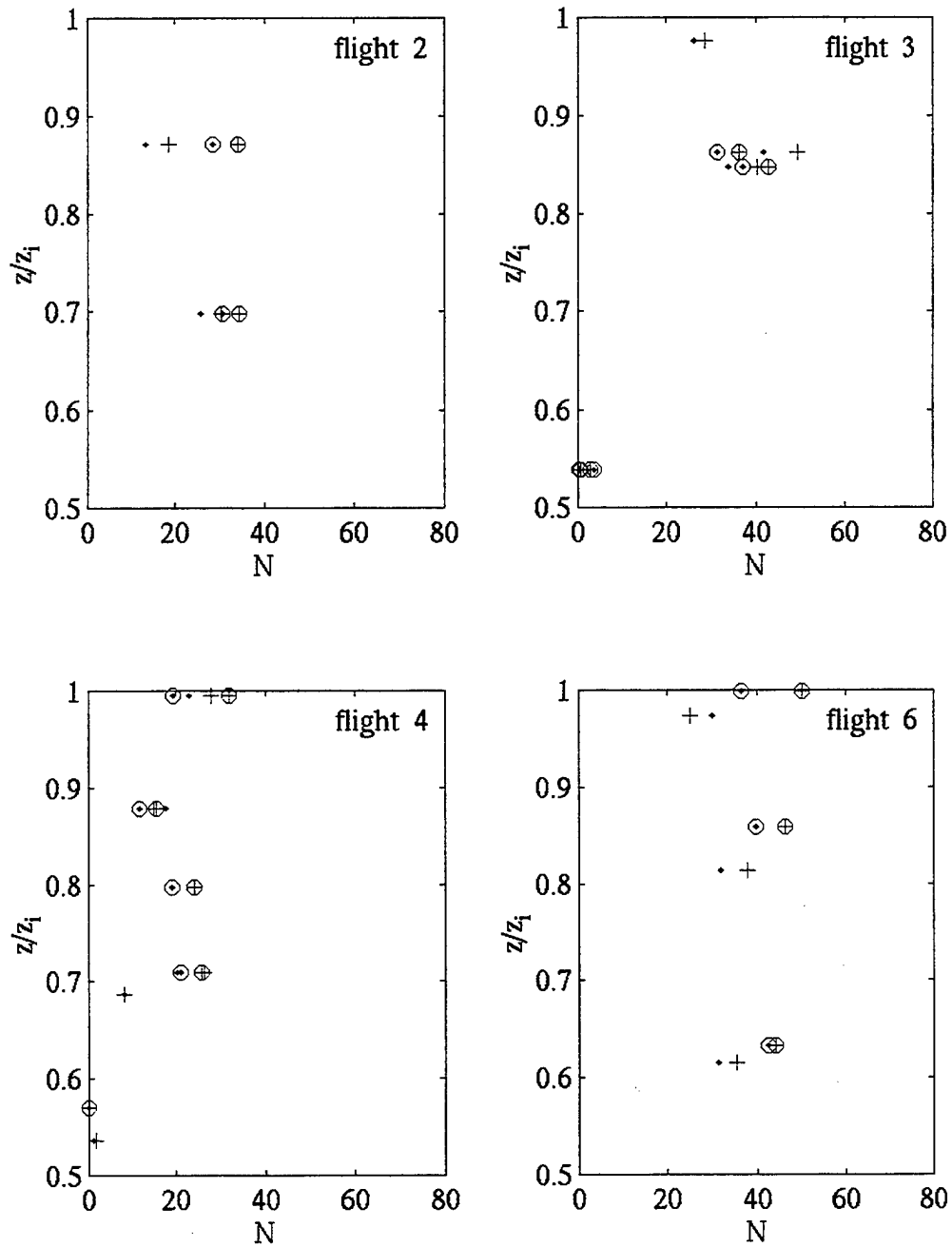


Figure 15, Continued.





**Figure 16.** Same as in Figure 9, Except for Number Concentration of Cloud Droplets (in  $\text{cm}^{-3}$ ).

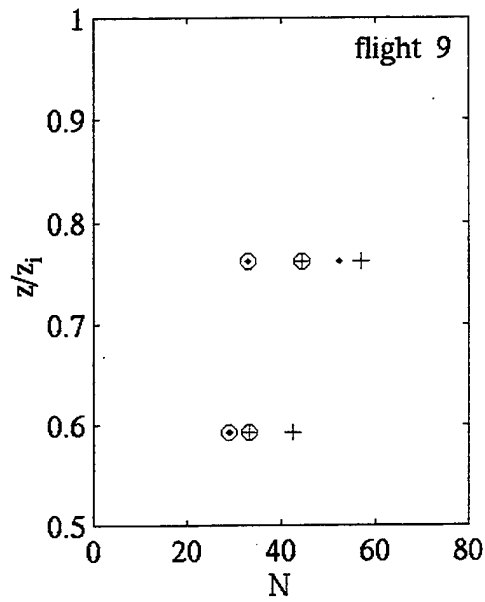
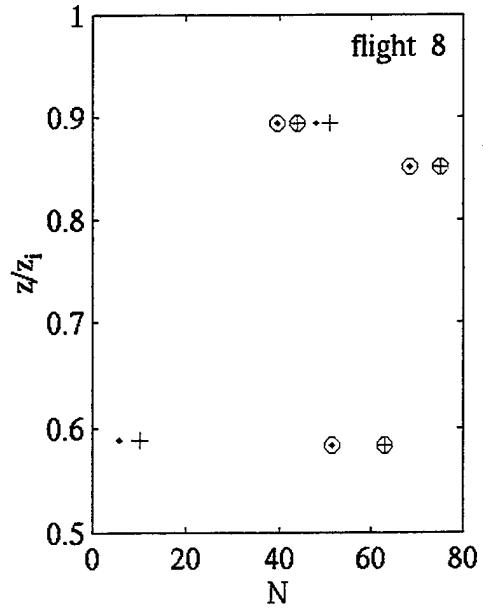
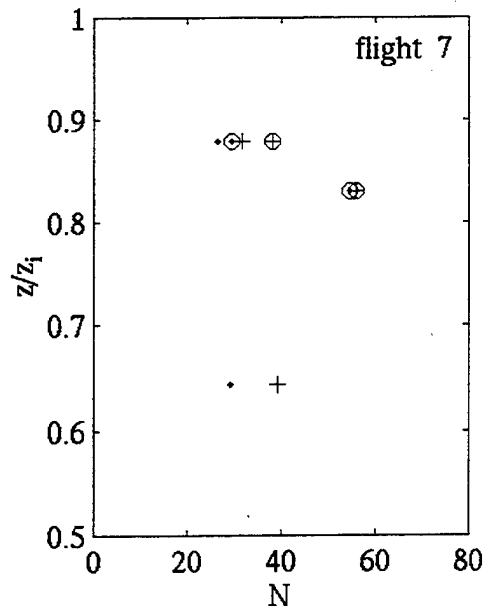


Figure 16, Continued.

## 2. Cloud Droplet Spectra

Many past studies indicate strong vertical and horizontal variations of cloud droplet spectra in marine stratocumulus due to various reasons. Martin et al. (1995), for example, indicated the effects of cumulus penetration on cloud microphysics. Noonkester (1984) observed horizontal variability in the droplet spectra of a stratus layer off of the southern California coast, attributing the variability to the horizontal variation in vertical mixing and relative humidity. Using large eddy simulations as a tool, Kogan et al. (1995) suggest that the cloud microphysical properties are significantly affected by BL dynamics, and that the cloud microstructure is significantly asymmetric between updrafts and downdrafts, especially near the cloud top and base. Their results suggest that 'natural' horizontal variability, associated with convective events, exists in all stratocumulus. However, such natural variability has not been analyzed from observations, although it is extremely important to the understanding of cloud formation/dissipation processes.

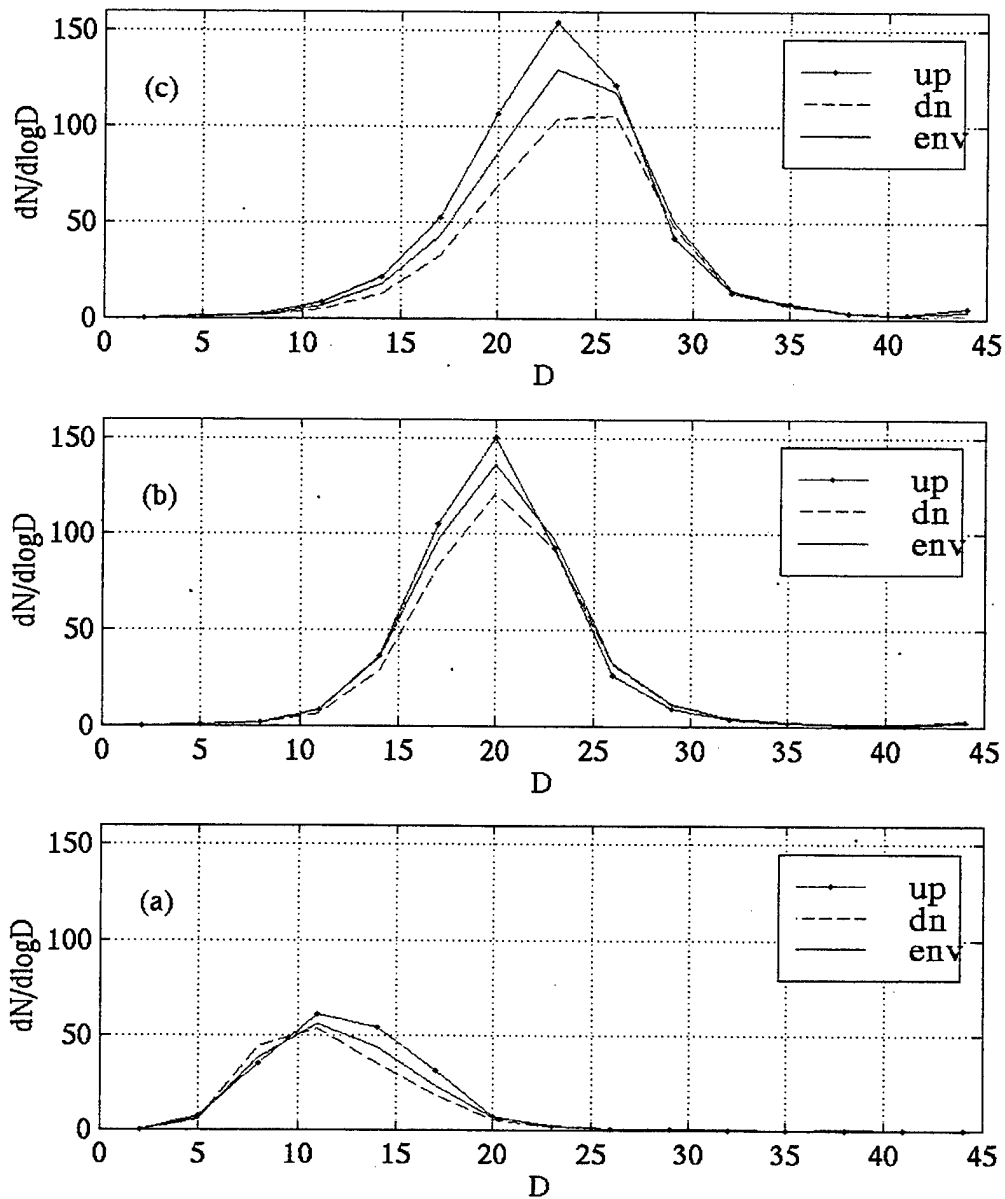
The integrated microphysical properties, such as the liquid water content, droplet volume diameter, and the number concentrations, were discussed in the previous sections. This section will focus on the variability in the droplet spectra. The results will be consolidated through consistency among different flights.

Some consistency is seen in the changes in droplet spectra with height within the stratocumulus cloud deck. Figure 17 shows an example of the mean droplet spectra in the convective updrafts and downdrafts at three representative levels in the cloud layer. The results are

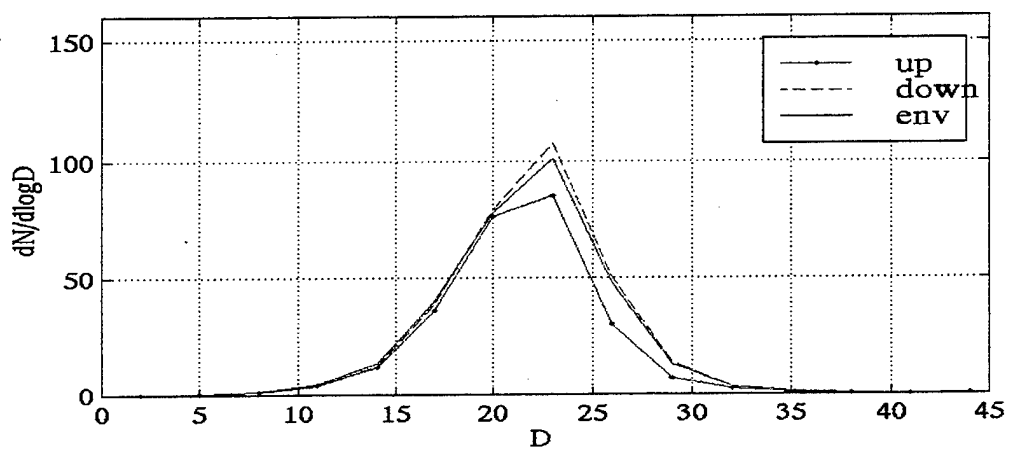
from flight 6, but are typical of those observed during FIRE. The droplet spectra in panels a, b, and c in Figure 17 were obtained from measurement legs near the cloud base, in the middle of the cloud layer, and near the cloud top, respectively.

Figure 17 shows the increase in droplet modal size from the cloud base to the cloud top. Integration of the spectra will naturally result in the increase in mean droplet diameter shown in Figure 14. It is seen in Figure 17 that the updrafts contain a larger concentration of droplets than the downdrafts, with the droplet spectra of the defined environment falling in between the updraft and downdraft droplet spectra. The difference in peak droplet concentration appears to increase towards the upper cloud layer. Near the top, the shape of the droplet spectra in updrafts and downdrafts seem to deviate rather significantly, with significant reduction in the number of small droplets occurring in the downdrafts. The large droplets do not appear to be affected. Such change in the shape of the droplet spectra result in larger mean droplet diameter in the downdrafts, as seen in Figure 14.

Strong horizontal variability on a scale of tens of kilometers is also observed in most of the flights analyzed in this study. Figure 18 shows the mean droplet spectra in the convective events from a different segment of the same cloud top turbulence leg in flight 6, shown in Figure 17c. Here, the total number concentration is significantly less although the modal droplet size is nearly the same. In addition, the downdrafts have a larger droplet number concentration than the updrafts, the exact opposite to the droplet spectra shown in Figure 17c. The reduction in total



**Figure 17.** Cloud Droplet Spectra from Three in-cloud Measurement Legs in Flight 6. The vertical axis is  $dN/d\log D$ , where  $N$  is the droplet number concentration (in  $\text{cm}^{-3}$ ) and  $D$  is the droplet diameter (in  $\mu\text{m}$ ). a) near the cloud base, b) near the middle of the cloud, c) near the cloud top. The symbols for updrafts, downdrafts, and the defined environment are given in the legend.



**Figure 18.** Same as Figure 17, Except for a Different Segment of the Same Turbulence Leg as in Figure 17c.

droplet number (while retaining the shape of the spectra) compared to the other time segment of the same measurement leg (Figure 17c) appears to indicate inhomogeneous entrainment mixing, as discussed in Baker et al. (1980). It is not clear, though, whether the change in the size spectra in the updraft and downdraft events is typical and what caused this change. With the limitations of *in situ* observations, the answer to these questions may have to come from large eddy simulations involving explicit cloud microphysics.

Figure 19 shows the droplet size distribution from two different turbulence legs from flight 3 that were flown in-cloud near the cloud base. Figure 19a has a spectral shape similar to the typical case in Figure 17, yet the plot indicates that the droplet concentration is largest in the defined environment, slightly higher than the updraft concentration. This implies that the turbulence is not as active in this region of the cloud base. As a result, the turbulence updraft and downdraft may not be well correlated with the activation and growth of the cloud droplets. Figure 19b shows a bimodal size distribution, with a larger concentration and smaller droplets in the updrafts in both modes. This spectral structure indicates that, in this well-mixed turbulent BL, there are downdraft droplets being recaptured and recycled in the updrafts at this particular horizontal location near the cloud base. This phenomenon was reproduced in a large eddy simulation model by Kogan et al. (1995).

We observed horizontal variability in the cloud droplet spectra in the cases where cumulus clouds penetrate the stratocumulus deck from below. Figure 20 illustrates one example of this occurrence in the FIRE flights using

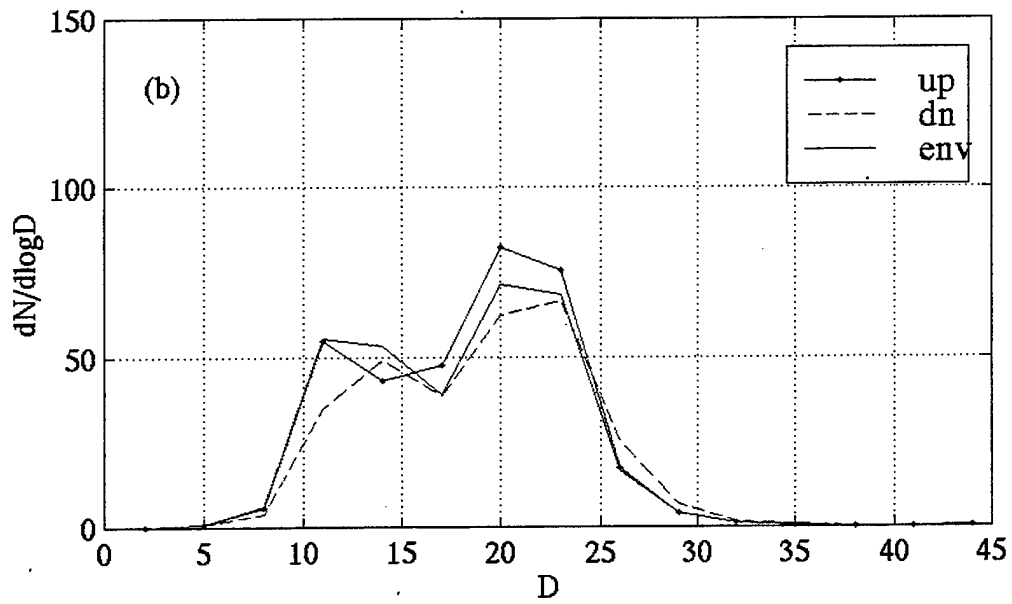
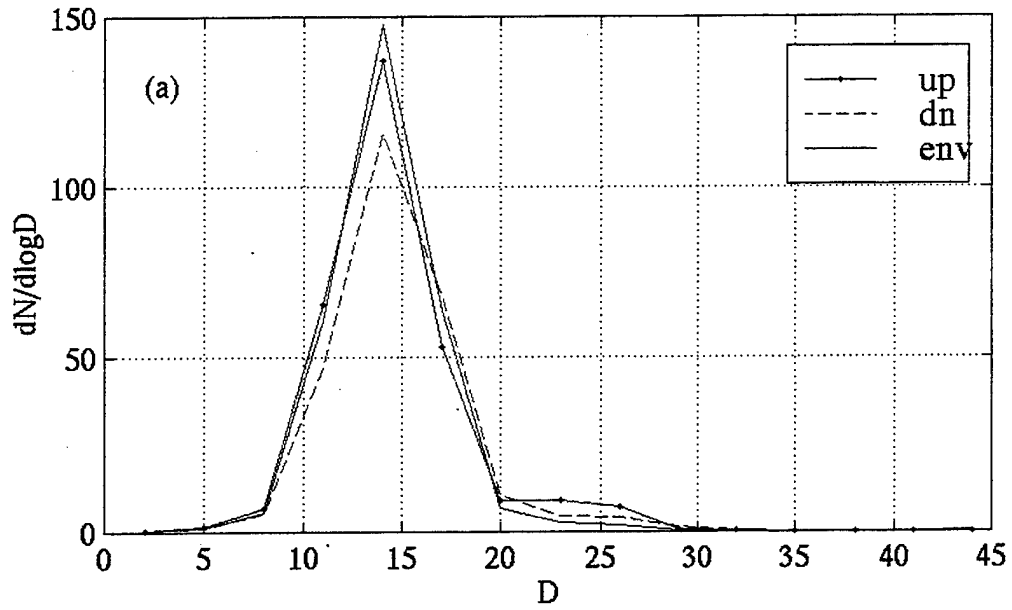


**Figure 19.** Same as in Figure 17, Except for Two Horizontal Turbulence Legs Near the Cloud Base in Flight 3. Legs are between 60 and 85 km apart.



measurements from flight 7. Figure 20 shows two cloud droplet spectra from the same horizontal measurement leg near the cloud top. During this in-cloud flight leg, the observer's notes indicate the presence of thick stratocumulus, with some regions of penetrating cumulus observed. The droplet spectra from the first segment (Figure 20a) appear similar to those shown earlier for flight 6 for the updrafts, downdrafts, and defined environment, and thus it is consistent with the droplet spectra of stratocumulus with no penetrating cumulus (Figure 17). In Figure 20b, however, the total number concentration is much higher, and the updraft and downdraft concentration is much higher than that of the defined environment. Also, the droplet sizes are smaller than those in Figure 20a. This is consistent with the findings of Martin et al. (1994), who observed that the intrusion of cumulus clouds resulted in a localized increase in droplet concentration and liquid water content in the stratocumulus layer, with a localized decrease in droplet size as more droplets compete for available water vapor.

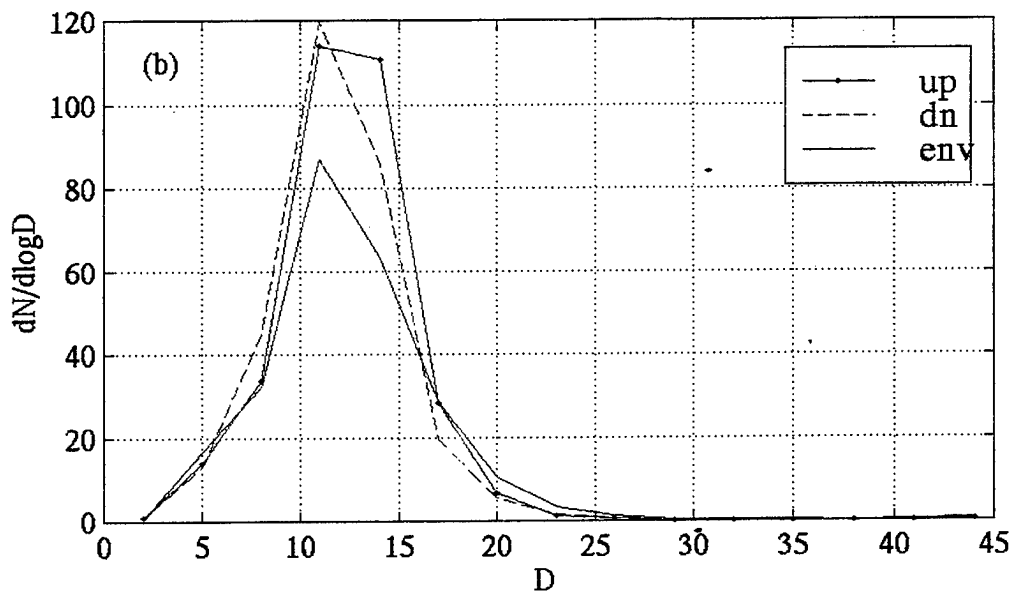
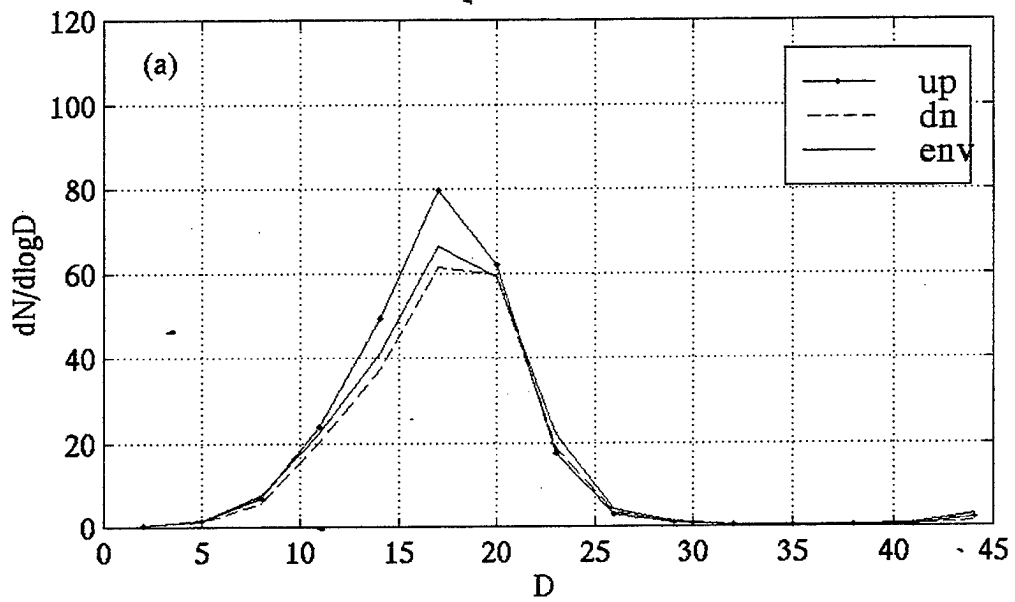


**Figure 20.** Same as Figure 19, Except for Flight 7 Where Penetration of the Stratocumulus by Cumulus was Observed. Cumulus penetration was recorded by the in-flight observer in (b).

### C. CONVECTIVE MASS FLUX PARAMETERIZATION

Betts (1975) developed the mass flux parameterization originally used to describe vertical flux transport in cumulus clouds. Betts (1978) later extended this to describe convection in the sub-cloud layer. The mass flux parameterization was originally developed to represent the vertical flux transport using the properties of the convective elements only. The parameterization applied to clear convective BL rather successfully (e.g., Khalsa and Greenhut (1985) and Greenhut and Khalsa (1987), for the trade wind cumulus BL, and Young (1988), for the clear convective BL). It is not clear, though, whether such parameterizations can be applied to the cloudy BL, as the convective activity in the cloudy BL is weaker and the contrast between the updrafts and downdrafts is in general smaller in the cloudy case.

In this parameterization from Betts (1978), fluxes of dry and moist static energy are represented by the product of a convective mass flux,  $\omega^*$ , and the difference between properties inside and outside convective elements,

$$\overline{w'x'} = \omega_x^*(x_u - x_d) \quad (7)$$

where  $\omega_x^*$  is the convective mass flux associated with the quantity  $x$ , and  $x_u$  and  $x_d$  are the conditionally averaged value of  $x$  for updrafts and downdrafts, respectively. Here, Equation (7) is tested using the observations from the seven FIRE flights in stratocumulus clouds. The convective mass flux,  $\omega^*$ , is calculated using the buoyancy flux, water

vapor flux, liquid water flux, and ozone flux from the horizontal turbulence legs at different levels within the BL. The results of the  $\omega^*$  calculations are shown in Figure 21. The calculations using the ozone flux from flight 9 were omitted due to a malfunction of the Model Mark II ozone sensor during that flight.

The results show a fair amount of consistency between the values of  $\omega^*$  calculated from the different fluxes. There is some scatter in the data points, the least amount of scatter being seen in the well-mixed cases of flights 3, 4 and 6, where the fluxes throughout the entire BL are rather strong. In these three flights, there is a trend of increasing  $\omega^*$  with height in the lower one third of the BL. In the upper two thirds of the BL,  $\omega^*$  remains fairly constant with the exception of flight 3 near the cloud top. Near the surface,  $\omega^*$  averages about  $0.2 \text{ ms}^{-1}$ , then increases to about  $0.3$  to  $0.4 \text{ ms}^{-1}$  in the upper BL. This trend for  $\omega^*$  can also be seen, though not as clearly, in the decoupled cases of flights 7 and 8. The results for flights 2 and 9 have significant scatter at various levels in the BL and do not show a clear trend. The values and variation of the calculated convective mass flux with height are similar to those obtained by and Khalsa and Greenhut (1985) and Greenhut and Khalsa (1987), who calculate  $0.15 < \omega^* < 0.25$  for latent heat, sensible heat, and along-wind momentum fluxes.

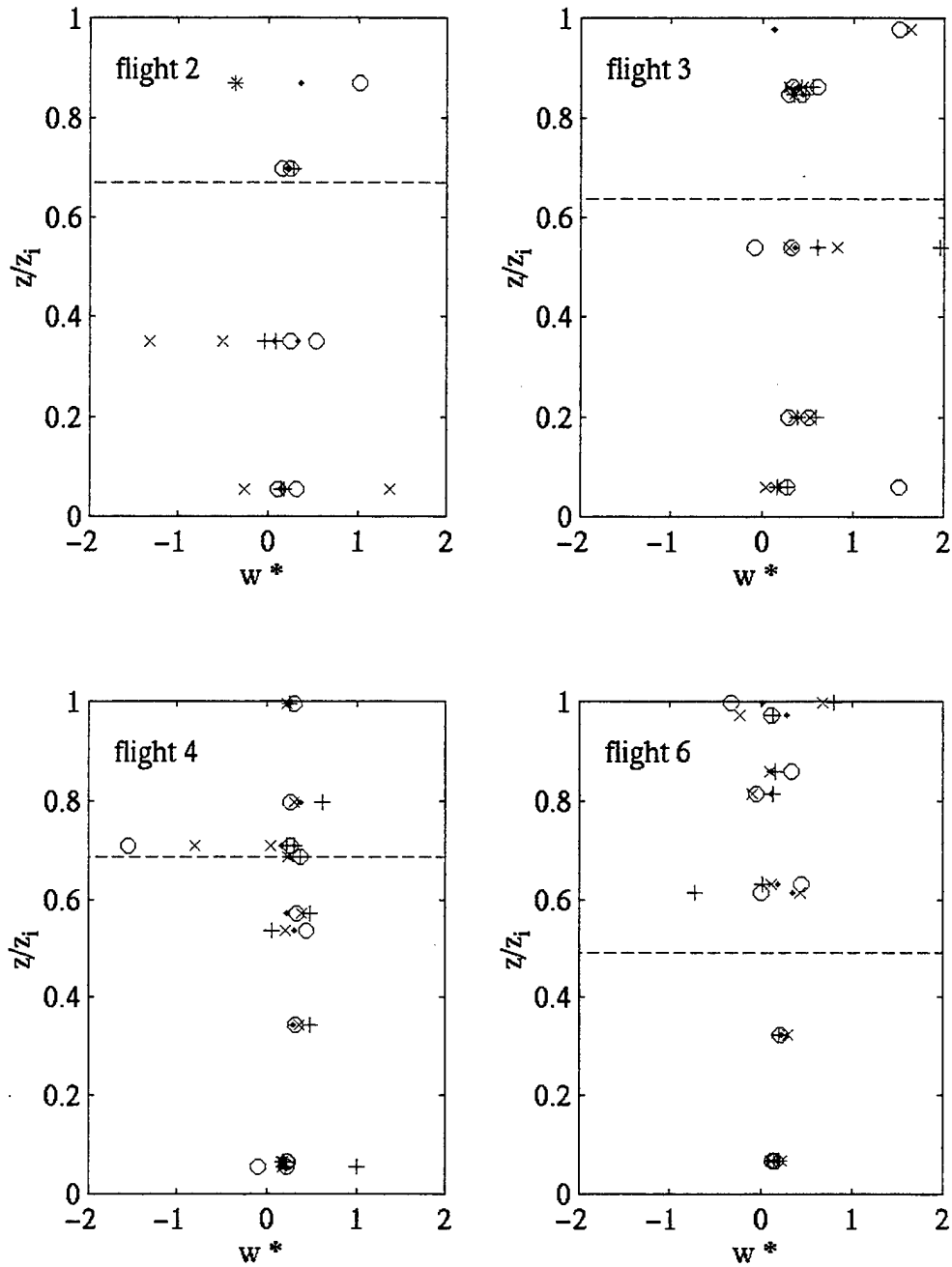


**Figure 21.** Convective mass flux,  $w^*$  (in  $\text{ms}^{-1}$ ) as a Function of Height Scaled by the BL Depth. Fluxes corresponding to each symbol are:  $\theta_v$  (+),  $q_v$  (·),  $q_1$  (o), and  $\text{O}_3$  (x). The dotted line shows the average height of the cloud base.

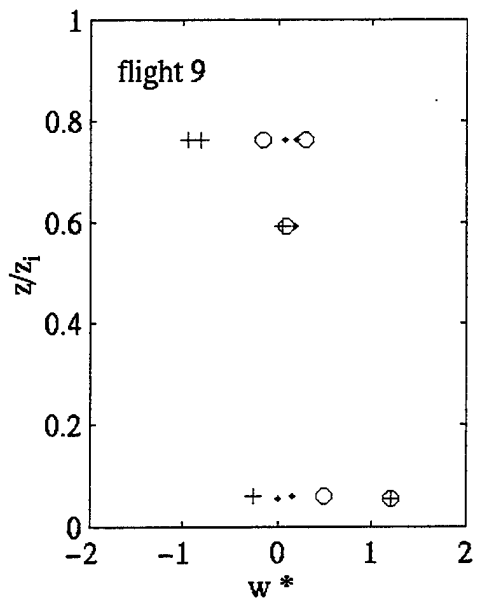
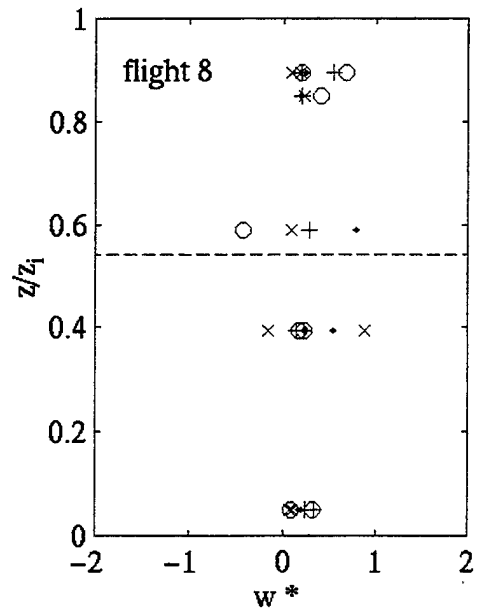
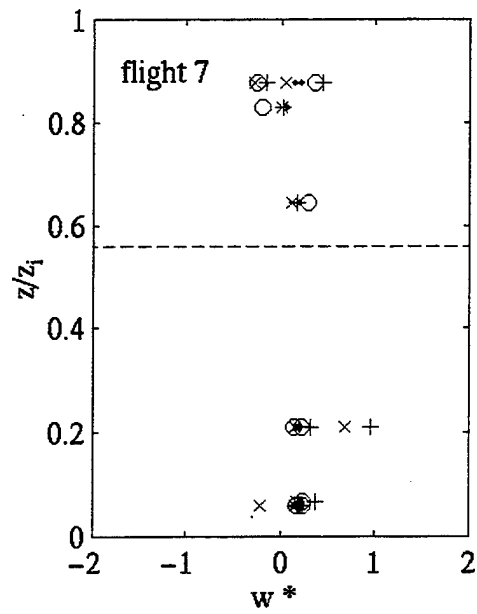


Figure 21, Continued.

## V. SUMMARY, CONCLUSIONS, AND DISCUSSION

### A. SUMMARY AND CONCLUSIONS

The overall objective of this thesis was to better understand the convective nature of the stratocumulus-topped boundary layer. This study used data collected by the NCAR Electra during seven of the FIRE flights. Of the seven flights analyzed in this study, three were determined to be well-mixed, three were decoupled, and one was uncertain.

We used a conditional sampling method to identify the turbulent updrafts and downdrafts in the horizontal turbulence legs at different levels within and below cloud. We selected minimum event width and vertical velocity criteria based on analysis of the data prior to the conditional sampling and also on the criteria used in Nicholls (1989), and investigated the geometric characteristics and leg-averaged properties of thermodynamic and microphysical quantities within the updrafts and downdrafts.

An in-depth analysis of the geometric properties of the convective events revealed some consistent trends. The vertical variation in the event size in the well-mixed BL cases was observed to increase steadily with height compared to the decoupled cases, where event size remained fairly constant up to about  $0.4z_I$ , suggesting that decoupling indeed suppresses the growth of the convective events. The number frequency of events was observed to be smallest in the upper BL in all flights. This decrease in the upper BL seems to correlate with the increase in the event size. The trends in the vertical variation of fractional area occupied

by updrafts and downdrafts are related to the strength of turbulence at each level in the BL. Stronger turbulence implies a greater area occupied by updrafts and downdrafts.

We observed great consistency in the analysis of many of the thermodynamic quantities in the updrafts and downdrafts. The mean vertical velocity in both the updrafts and downdrafts for all flights is fairly symmetrical with height in the BL. Flight 3, the well-mixed, nocturnal case containing strong radiative and evaporative forcing, had the strongest convective events. Large water vapor perturbations were observed near the sea surface (moisture source) and cloud top (warm, dry air source), with minimum values generally seen in the cloud mixed layer away from the cloud boundaries. Both updrafts and downdrafts showed a consistent trend of increasing liquid water content with height in the cloud layer. The fractional difference in liquid water content between updrafts and downdrafts was also consistently positive, with the largest positive liquid water differences occurring near the cloud base, consistent with activation of cloud droplets in the updrafts here. We observed less consistency in the virtual potential temperature perturbation (or buoyancy excess) profiles, which varied greatly among the flights. This variability is likely the result of the variation in cloud top and surface forcing between the different cases. The average inversion jump conditions for the FIRE flights from McDowell (1999) were applied to the buoyancy reversal criterion of Siems et al. (1990). The buoyancy reversal criterion was satisfied in all seven flights, suggesting that the cool downdrafts identified in the upper boundary layer are likely a result of both radiative cooling and evaporative cooling.



Analysis of updraft/downdraft microphysical parameters revealed consistent trends as well. In nearly all of the flights, the downdrafts contain fewer and larger droplets while the updrafts contain more and smaller droplets, consistent with droplet formation and growth in the updrafts and evaporation due to entrainment drying in the downdrafts.

Both vertical and horizontal variability were observed in the updraft and downdraft cloud droplet spectra from the FIRE flights. As already noted, the updrafts typically contain a larger concentration of droplets at all droplet size bins than the downdrafts for a given in-cloud leg. Additionally, the droplet spectra of the defined environment falls in between the updraft and downdraft droplet spectra, and there is typically no shift in the peak droplet size between the updrafts, downdrafts, and environment at a given height. There is a shift to larger droplet sizes with increasing height in the cloud, independent of the convective events. The difference in peak droplet concentration between updrafts, downdrafts, and environment appears to increase near the cloud top. Additionally, the number of small droplets occurring in the downdrafts appears to decrease near the cloud top, resulting in the observed larger mean droplet diameters in the downdrafts here. In most of the flights analyzed, we observed significant differences in the droplet spectra between two legs at the same vertical level in a particular flight, indicating the horizontal variability of the cloud microstructure on a scale larger than the boundary layer internal circulation (50 to 100 km). The differences seen are likely the result of localized changes in the extent of turbulent mixing occurring near the cloud top and base and also the

interaction with cumulus forming beneath the stratocumulus deck in a localized area.

The validity of the mass flux ( $\omega^*$ ) parameterization, based on methods used in previous work for the clear convective BL by Betts (1975 and 1978), Khalsa and Greenhut (1985) and Greenhut and Khalsa (1987), was tested for the stratocumulus-topped BL. The results suggest that the parameterization is applicable to the FIRE data, especially in the cases of stronger turbulence where there is less scatter among the values of  $\omega^*$  calculated using different fluxes. Near the surface,  $\omega$  averages about  $0.2 \text{ ms}^{-1}$ , then increases to about  $0.3$  to  $0.4 \text{ ms}^{-1}$  in the upper BL, which is comparable to values obtained by and Khalsa and Greenhut (1985) and Greenhut and Khalsa (1987).

## **B. DISCUSSION**

This study has looked closely at the convective structure of the BL using calculations based on data from observations. We do not present error statistics for the calculations of the convective event mean profiles, geometric properties, and droplet spectra made in this study. In one aspect, there is no accepted method of error representation for these types of calculations. Nevertheless, confidence in the results is obtained through consistency between results from different flights.

The geometric and thermodynamic properties identified from this study are also supported by the work of other researchers using other datasets. The current research provides, for the first time, the microphysical properties in the convective events. These observational results are

consistent with those from large eddy simulations with explicit cloud microphysics, such as in Kogan et al. (1995). The differences in the microphysical properties between the turbulent updrafts and downdrafts clearly revealed the physical processes occurring in each type of event. More well-designed in-cloud measurements are desirable to further quantify the findings here. Furthermore, this study clearly identified the differences in the event properties between the well-mixed cases and the decoupled cases. These results should be quantified with more cases in each category to achieve high statistical significance.

THIS PAGE INTENTIONALLY LEFT BLANK

## LIST OF REFERENCES

- Albrecht, B. A., D. A. Randall and S. Nicholls, 1988: Observations of marine stratocumulus during FIRE. *Bull. Amer. Meteor. Soc.*, **69**, 618-626.
- Baker, M.B., R.G. Corbin, and J. Latham, 1980: The influence of entrainment on the evolution of cloud droplet spectra. I: A model of inhomogenous mixing. *Quart. J. Roy. Meteor. Soc.*, **106**, 581-598.
- Betts, A.K., 1975: Parametric interpretation of trade-wind cumulus budget studies. *J. Atmos. Sci.*, **32**, 1934-1945.
- \_\_\_\_\_, 1978: Convection in the tropics. *Meteorology Over the Tropical Ocean*, D.B. Shaw Ed., Royal Meteor. Soc., pp. 105-132.
- Cox, S. K., D. McDougal, D. Randall, and R. Schiffler, 1987: FIRE- The first ISCCP Regional Experiment. *Bull. Amer. Meteor. Soc.*, **68**, 114-118.
- Deardorff, J. W., 1980: Cloud-top entrainment instability. *J. Atmos. Sci.*, **37**, 131-147.
- Fravalo, C., Y. Fouquart, and R. Rosset, 1981: The sensitivity of a model of low stratiform clouds to radiation. *J. Atmos. Sci.*, **38**, 1049-1062.
- Gerber, H., 1996: Microphysics of marine stratocumulus clouds with two drizzle modes. *J. Atmos. Sci.*, **53**, 1649-1662.
- Greenhut, G.K., and S.J.S. Khalsa, 1987: Convective elements in the marine atmospheric boundary layer. Part I: conditional sampling statistics. *J. Climate Appl. Meteor.*, **26**, 813-822.
- Khalsa, S.J.S., 1993: Direct sampling of entrainment events in a marine stratocumulus layer. *J. Atmos. Sci.*, **50**, 1734-1750.
- Khalsa, S.J.S and G.K. Greenhut, 1985: Conditional sampling of updrafts and downdrafts in the marine atmospheric boundary layer. *J. Atmos. Sci.*, **42**, 2550-2562.

Kloesel, K. A., B. A. Albrecht and D. P. Wylie, 1988: FIRE marine stratocumulus observations ---- summary of operations and synoptic conditions. FIRE Tech. Rep. NO.1, The Pennsylvania State University, Dept. of Meteorology, University Park.

Kogan, Y.L., M.P. Khairoutdinov, D.K. Lilly, Z.N. Kogan, and Qinfu Liu, 1995: Modeling of stratocumulus cloud layers in a large eddy simulation model with explicit microphysics. *Amer. Meteor. Soc.*, **52**, 2923-2940.

Laufersweiler and Kloesel, 1991: FIRE marine stratocumulus observations --- vertical structure of the marine atmospheric boundary layer. FIRE Technical Report No. 3, Pennsylvania State University, Dept. of Meteorology, University Park, PA.

Lenschow, D.H., and P.L. Stephens, 1980: The role of thermals in the convective boundary layer. *Bound-Layer Meteor.*, **19**, 509-532.

\_\_\_\_\_ and \_\_\_\_\_, 1982: Mean vertical velocities and turbulence intensity inside and outside thermals. *Atmos. Environ.*, **16**, 761-764.

Manton, M.J., 1977: On the structure of convection. *Bound.-Layer Meteor.*, **12**, 491-503.

Martin, G.M., D.W. Johnson, D.P. Rogers, P.R. Jonas, P. Minnis, and D.A. Hegg, 1995: Observations of the interaction between cumulus clouds and warm stratocumulus clouds in the marine boundary layer during ASTEX. *J. Atmos. Sci.*, **52**, 2902-2922.

McDowell, D. W., 1999: Determining entrainment rate and the role of entrainment in stratocumulus clouds. Master's Thesis, Naval Postgraduate School, Dept. of Meteorology, Monterey, CA. 62 pp.

Nicholls, S., 1984: The dynamics of stratocumulus: aircraft observations and comparisons with a mixed layer model. *Quart. J. Roy. Meteor. Soc.*, **110**, 783-820.

Nicholls, S., and J. Leighton, 1986: An observational study of the structure of stratiform cloud sheets: Part I. Structure. *Quart. J. R. Meteor. Soc.*, **112**, 431-460.

- Nicholls, S., 1989: The structure of radiatively driven convection in stratocumulus. *Quart. J. Roy. Meteor. Soc.*, **115**, 487-511.
- Noonkester, V.R., 1984: Droplet spectra observed in marine stratus cloud layers. *J. Atmos. Sci.*, **41**, 829-845.
- Randall, D.A., 1980: Conditional Instability of the first kind upside-down. *J. Atmos. Sci.*, **37**, 125-130.
- Rogers, D.P., and J.W. Telford, 1986: Metastable stratus tops. *Quart. J. R. Meteor. Soc.*, **112**, 481-500.
- Rogers, D. P., C. E. Dorman, K.A. Edwards, I.M. Brooks, W. K. Melville, S. D. Burk, W. T. Thompson, T. Holt, L. M. Storm, M. Tjernstrom, B. Grisogono, J. M. Bane, W. A. Nuss, B. M. Morley, and A.J. Schanot, 1998: Highlights of Coastal Waves 1996, *Bull. Amer. Meteorol. Soc.*, **79**, 1307-1326.
- Siems, S.T., C.S. Bretherton, M.B. Baker, S. Shy, and R.T. Breidenthal, 1990: Buoyancy reversal and cloudtop entrainment instability. *Quart. J. Roy. Meteor. Soc.*, **116**, 705-739.
- Stull, R. B., 1988: *An Introduction to Boundary Layer Meteorology*, Kluwer Academic Publishers, Dordrecht, The Netherlands.
- Wang, Q., 1993: Turbulent mixing and transport in marine stratocumulus-topped boundary layers--an observational study. Ph.D. dissertation, Department of Meteorology, The Pennsylvania state University, University Park, PA 199 pp.
- Wang, Q., and B. A. Albrecht, 1994: Observations of cloud-top entrainment in marine stratocumulus clouds. *J. Atmos. Sci.*, **51**, 1530-1547.
- Wang, Q., 1996: Boundary layer turbulence structure observed during the Lagrangian measurements in ASTEX, Proceedings of the ETL/CSU Cloud-Related Process Modeling and Measurement Workshop, Boulder, Colorado, 23-25 October 1995, 163-174.
- Wang, S., and D.H. Lenschow, 1995: an observational study of the role of Penetrating cumulus in a marine stratocumulus-topped boundary layer. *J. Atmos. Sci.*, **52**, 2778-2787.

Young, G.S., 1988: Turbulence structure of the convective boundary layer. Part II: Phoenix 78 aircraft observations of thermals and their environment. *Amer. Meteor. Soc.*, **45**, 727-735.



**INITIAL DISTRIBUTION LIST**

|   | No. Copies |
|---|------------|
| 1. Defense Technical Information Center.....2<br>8725 John J. Kingman Road, STE 0944<br>Ft. Belvoir, Virginia 22060-6218                |            |
| 2. Dudley Knox Library.....2<br>Naval Postgraduate School<br>411 Dyer Rd.<br>Monterey, California 93943-5101                            |            |
| 3. Chairman, Code MR.....1<br>Department of Meteorology<br>Naval Postgraduate School<br>Monterey, California 93943-5101                 |            |
| 4. Chairman, Code OC.....1<br>Department of Oceanography<br>Naval Postgraduate School<br>Monterey, California 93943-5101                |            |
| 5. Professor Qing Wang, Code MR/Qg.....3<br>Naval Postgraduate School<br>Monterey, California 93943-5101                                |            |
| 6. Professor Peter S. Guest, Code MR/Gs.....1<br>Naval Postgraduate School<br>Monterey, California 93943-5101                           |            |
| 7. Commander.....1<br>Naval Meteorology and Oceanography Command<br>1020 Bach Boulevard<br>Stennis Space Center, Mississippi 39529-5005 |            |
| 8. LT Michelle K. Whisenant, Code 35.....2<br>Naval Postgraduate School<br>Monterey, California 93943-5101                              |            |